Disjoining pressure in thin liquid foam and emulsion films—new concepts and perspectives



2003 J. Phys.: Condens. Matter 15 R1197

(http://iopscience.iop.org/0953-8984/15/27/201)

INSTITUTE OF PHYSICS PUBLISHING JOURNAL OF PHYSICS: CONDENSED MATTER

J. Phys.: Condens. Matter **15** (2003) R1197–R1232 PII: S0953-8984(03)57066-7

**TOPICAL REVIEW**

# Disjoining pressure in thin liquid foam and emulsion films—new concepts and perspectives

**Cosima Stubenrauch**[1,3] **and Regine von Klitzing**[2]

[1] Institut für Physikalische Chemie, Universität zu Köln, Luxemburger Straße 116, D-50939 Köln, Germany
[2] Stranski-Laboratorium, TU Berlin, Strasse des 17 Juni 112, D-10623 Berlin, Germany

E-mail: stubenrauch@uni-koeln.de

Received 3 December 2002
Published 27 June 2003
Online at stacks.iop.org/JPhysCM/15/R1197

**Abstract**

The present review is a topical survey of the disjoining pressure in thin liquid foam and emulsion films from both the experimental and the theoretical points of view. Section 2 deals with the latest research work on experimental techniques with which the disjoining pressure $\Pi$ in foam, emulsion, and pseudo-emulsion films can be measured. Although a lot of techniques are available, the question of the origin of the charges at the water/air and the water/oil interfaces of films, which are stabilized by non-ionic surfactants, has not yet been answered. We address this question in section 3, reviewing the latest relevant literature. The relevance of structural forces for the disjoining pressure is outlined in section 4, which focuses on films which are stabilized by surfactant/polyelectrolyte mixtures.

(Some figures in this article are in colour only in the electronic version)

## Contents



[3] Author to whom any correspondence should be addressed.

  

## 1. Introduction

Foams and emulsions are dispersions of two phases. In the case of (liquid) foams the dispersed phase is a gas (e.g. air) and the continuous phase is a liquid (e.g. an aqueous surfactant solution), whereas emulsions consist of two liquid phases (e.g. oil and water). The continuous phase forms a film between two bubbles or drops of the dispersed phase. The stability of these films affects the stability of the whole system, which itself is interesting for many technical applications. To understand the macroscopic stability it is necessary to understand the properties of the building blocks, i.e. the single films. Therefore, single foam and emulsion films have been of great interest in basic research for several decades.

### *1.1. Forces in thin liquid films*

In foams and emulsions the pressure in the dispersed phase ($P_d$) is higher than the pressure in the surrounding liquid ($P_l$), so a capillary suction occurs. The pressure difference $\Delta P = P_d - P_l$ is related to the radius $r$ of the dispersed bubbles or droplets according to the Laplace equation $\Delta P = P_c = 2\sigma/r$. $P_c$ is the so-called capillary pressure and $\sigma$ the interfacial tension of the continuous phase. The drainage of the intermediate thin films induced by $P_c$ is slowed down and eventually prevented when interactions between the film surfaces come into play. These interactions are called the disjoining pressure $\Pi$. This pressure acts perpendicular to the interfaces, thus balancing the pressure difference $\Delta P$, i.e. the capillary pressure $P_c$. A quasi-static situation is reached when $P_c$ equals the disjoining pressure $\Pi$. The disjoining pressure is due to interaction forces between the two interfaces of the thin liquid film. These forces are very well reviewed in [1]. One usually defines the disjoining pressure as the sum of long-range repulsive electrostatic ($\Pi_{elec}$), short-range attractive van der Waals ($\Pi_{vdW}$) and short-range repulsive steric ($\Pi_{steric}$) pressures. A sketch of the resulting $\Pi(h)$ curve (the dependence of the joining pressure on the film thickness) is shown in figure 1. Note that not all regions of the $\Pi(h)$ curve are stable. If $\Pi$ decreases with decreasing $h$, the film thins until either $\Pi$ increases again or the film ruptures. In the former case two stable regions of different thickness can be distinguished. As can be seen in figure 1, the thick *common black films* (CBF) are mainly stabilized by electrostatic double-layer forces, whereas in the thin *Newton black films* (NBF) the stability is determined by entropic confinement forces [1, 2].

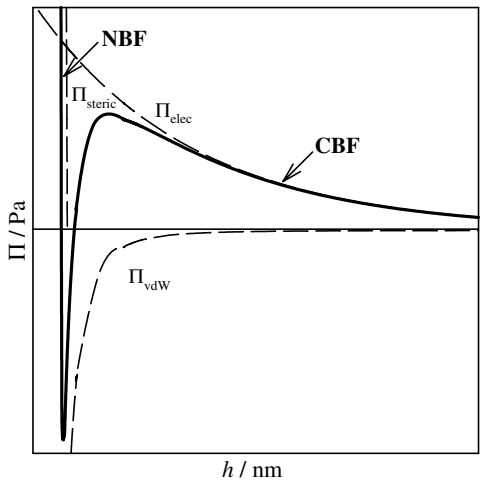


**Figure 1.** A schematic representation of the disjoining pressure Π as a function of the film thickness $h$ (solid curve). The three main contributions to Π are repulsive electrostatic ($\Pi_{elec}$), attractive van der Waals ($\Pi_{vdW}$), and repulsive steric ($\Pi_{steric}$) forces, each given by dashed curves. In the so-called CBF the stability is determined by $\Pi_{elec}$, whereas the NBF are stabilized by $\Pi_{steric}$.

### *1.2. Focus of the present review*

The behaviour of thin liquid films containing low-molecular-mass surfactants below the cmc is mainly determined by DLVO and steric forces. Examples of such films are given in section 3, where the influence of ionic and non-ionic surfactants is compared. In the last few years, the research activities have been extended to properties of more complex systems, where additional forces become important. For instance, the presence of aggregates, particles, or macromolecules in the films induces oscillatory structural forces under certain experimental conditions, which is shown in section 4. Furthermore, this review deals with the development of methods for investigating the interactions within liquid foam and emulsion films. A large number of methods are reviewed in section 2, most of which focus on techniques which are suitable for measuring the disjoining pressure in foam, emulsion, and pseudo-emulsion films.

## 2. Experimental developments and improvements

Section 2 is about the experimental developments and improvements in measuring the disjoining pressure of thin liquid films. In order to judge them, the most important aspects of the 'most popular' *thin-film pressure balance* (TFPB) technique will be summarized in section 2.1.1. Successful attempts to adapt this technique to emulsion and pseudo-emulsion films will be discussed and compared with alternative experimental methods.

### *2.1. Foam films*

#### *2.1.1. The 'most popular' TFPB.*

*General set-up:* The disjoining pressure Π can be measured as a function of the film thickness $h$ with a TFPB [1, 3–6]. With this technique free-standing horizontal liquid foam films with radii in the millimetre range can be investigated. To create these films a special film holder

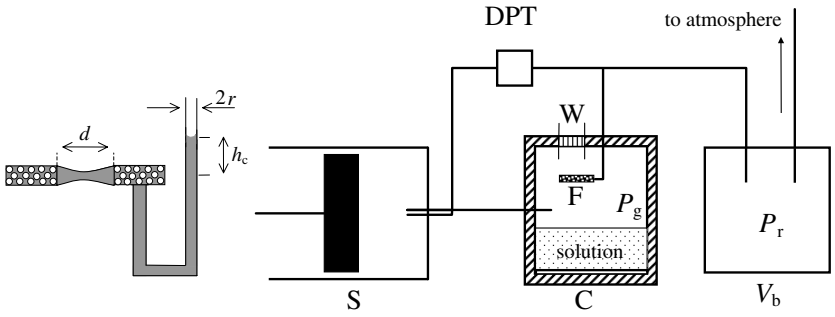


**Figure 2.** Left: the film holder consisting of a porous glass disc and a glass tube of radius $r = 1.5$ mm. The border of the fritted glass around the hole has a thickness of the order of 0.1 mm, $d$ is the diameter of the hole drilled through the disc (usually between 1 and 2 mm), and $h_c$ the height of the liquid in the tube. Right: a schematic picture of the TFPB. C is the measuring gas-tight cell with a window W in which the film holder F is placed such that the film is exposed to the gas pressure $P_g$ and the free end of the glass tube to the reference pressure $P_r$ (i.e. atmospheric pressure). The syringe S regulates $P_g$. The cell is filled with the surfactant solution to guarantee a saturated atmosphere. The pressure difference $P_g - P_r$ is measured by a DPT. With the buffer volume $V_b$, pressure fluctuations are minimized. Redrawn with permission from *PCCP* [11].

is used (figure 2, left). The film holder consists of a porous glass disc which is connected to a glass tube in such a way that the surfactant solution is free to move. The film is formed in a small hole with a diameter of 1–2 mm drilled through the disc. The film holder is placed in a cell where a constant gas pressure $P_g$ can be adjusted (figure 2, right). The $\Pi(h)$ curves are obtained while subjecting the liquid film to a defined gas pressure $P_g$ and measuring its equilibrium thickness $h$ interferometrically (see below).

*Determination of the disjoining pressure* $\Pi$*:* The disjoining pressure $\Pi$ can be calculated according to

$$\Pi = P_g - P_l = P_g - P_r + 2\sigma/r - \Delta\rho\, g h_c \tag{1}$$

where $P_l$ and $P_r$ are the liquid and the external reference pressures (i.e. atmospheric pressure), respectively, $\sigma$ is the surface tension of the surfactant solution, $r$ is the radius of the glass tube (in the millimetre range), $\Delta\rho$ the density difference between the surfactant solution and air, $g = 9.81$ m s$^{-2}$, and $h_c$ is the height of solution in the glass tube above the film (see figure 2, left). The pressure difference $\Delta P = P_g - P_r$ can be measured with an accuracy of $\pm 0.1\%$ by means of difference pressure transducers (DPT). For measurements at $\Pi$ values below 100 Pa, the parameters $\sigma$, $r$, $\Delta\rho$, and $h_c$ have to be determined accurately and pressure fluctuations in the cell have to be avoided. With the corresponding elaborate techniques, especially a precise measurement of $h_c$, the error of $\Pi$ can be reduced to $\pm 1$ Pa [5]. The accuracy of the disjoining pressure is mostly limited by the DPT, which has usually a specificity of 0.3% of its full range (i.e. 3–30 Pa).

*Determination of the film thickness* $h$*:* The thickness of the film is determined interferometrically. For this purpose, white light of intensity $I_0$ is directed perpendicularly to the flat portion of the film and the intensity of the reflected light $I$ is measured. To guarantee that shifts or fluctuations of $I_0$ do not influence the measured intensity $I$, the intensity $I$ and $I_0$ should be measured separately. Another possibility is to use a chopper which modulates the light amplitude with a low frequency. The intensity $I$ of the reflected light at a given

wavelength (usually 546 or 660 nm) is used to calculate the *equivalent* film thickness first suggested by Scheludko and Platikanov [7]:

$$h_{eq} = \frac{\lambda}{2\pi n_s} \arcsin\left(\frac{\Delta}{1 + (4R(1-\Delta)/(1-R)^2)}\right) \tag{2}$$

where $\lambda$ is the wavelength of the measured light, $n_s$ is the refractive index of the solution, $\Delta = (I - I_{min})/(I_{max} - I_{min})$, $R = (n_s - 1)^2/(n_s + 1)^2$, $I$ is the instantaneous intensity of the reflected light, and $I_{min}$ and $I_{max}$ correspond to the minimum and maximum values of the intensity. The thickness of the *equivalent* film with a homogeneous refractive index is calculated using equation (2). But in general the film is assumed to consist of three layers: an intermediate bulk layer of thickness $h_{bulk}$ and refractive index $n_{bulk}$ and two interfacial layers consisting of an adsorbed surfactant layer ($n_{tail}, n_{head}, h_{tail}, h_{head}$) [8]. The *physical* film thickness $h$ is related to the equivalent thickness by

$$h = h_{eq} - 2h_{tail}\left(\frac{n_{tail}^2 - n_s^2}{n_s^2 - 1}\right) - 2h_{head}\left(\frac{n_{head}^2 - n_s^2}{n_s^2 - 1}\right). \tag{3}$$

This correction is important for thin films (e.g. NBF, $h \sim 4$ nm). However, the determination of the refractive index and the thickness of the interfacial layers cannot be precise, since the surfactant density and the degree of hydration of the head-groups in the film are not directly accessible. Good estimates can be found for octyl glucoside $C_8G_1$ [9], the alkyl maltosides $C_{10}G_2$ [10] and $C_{12}G_2$ [11], and for the alkyl trimethylammonium bromides $C_n$TAB [12]. Together with the experimental uncertainties, an error of at least $\pm 5\%$ results for the film thickness $h$. However, the reproducibility of the data is often lower [10, 13, 14] especially for CBF at low surface charges. The lower the surface charge the higher the inaccuracy, which can be as high as $\pm 10\%$.

For the sake of completeness it has to be mentioned that a set-up was developed with which the thickness can be determined by using x-ray reflectivity [15–17]. According to the authors, the level of accuracy achieved with this apparatus is $\leqslant 0.1$ nm.

*Temperature control:* The majority of measurements are carried out at room temperature (20–23 °C) and an error of $\pm 1$ °C is always reported. Assuming that the adsorption of the surfactant at the water/air interface is not significantly influenced by the temperature and that no phase transition occurs in this temperature range, the interactions between the film interfaces are not affected by changes in temperature. This is due to nearly constant DLVO forces over a wide range of temperature. The experimental problem is not the control of the temperature itself but its homogeneity. Any temperature gradients in the measuring cell or along the capillary tube have to be avoided [18]. This is ensured if measurements are simply performed at room temperature without any further thermostating device (as for example in [11, 14, 19]). In some of the existing TFPBs only the jacket of the measuring cell is thermostated, whereas the cover and the glass tube of the film holder are exposed to room temperature [5, 20, 21]. In these cases, the temperature of the jacket always is (and has to be!) adjusted to room temperature. To our knowledge only one temperature-dependent measurement with such a set-up has been published [20]. In this study, the temperature of the laboratory was adjusted to the cell temperature in a range from 20 to 30 °C, a procedure that is not very convenient. However, temperature-dependent measurements are easily possible if the complete cell (including its top) consists of a metal which has a high heat conductivity (e.g. brass) [22]. In the top a quartz window is let in to enable interferometric measurements. Beside the cell and the top, also the window is heated to avoid condensation. The glass tube is directly connected to the metal top which facilitates a fast heat balance between the liquid

in the tube and the liquid within the film. Another possibility is to place the whole cell in a thermostating device (see for example figure 2.11 in [23]). Note that in [24] not only the cell but also the syringe with which the pressure is applied are placed in the thermostating device. Although only measurements in a range from 10 to 35 °C are published, with such a set-up more elevated temperatures should be accessible. A large temperature range is of interest for investigating the CBF–NBF transition [25] and phase transitions occurring inside the film or at its surface [20, 26, 27].

*2.1.2. Calibration.* An underestimated problem is the fact that the TFPB cannot be 'calibrated' in the usual sense because films of defined thickness and refractive index are not available for the nanometre range. In addition, the TFPB is not commercially available, i.e. all existing instruments are home-built. Thus, a 'standard' system has to be defined with which the same $\Pi(h)$ curves should be measured, whatever the experimental set-up. It has to be underlined that an 'accepted' standard would be very helpful as a lot of experimental difficulties can occur which could be overlooked without a point of reference. As a standard the cationic surfactant tetradecyl trimethylammonium bromide, $C_{14}$TAB, is proposed [11] as it is cheap, easy to purify, and forms stable films at concentrations around the cmc. Very good agreement was found between the $\Pi(h)$ curves of a 3.5 mM $C_{14}$TAB solution measured independently by different groups [11, 12]. It should be mentioned that the anionic surfactant sodium dodecyl sulfate (SDS) was used recently to calibrate a new type of film holder (see below) [28]. However, as it is known that the hydrolysis of SDS results in traces of dodecanol that influences the $\Pi(h)$ curves [5], it may be easier to take the non-hydrolysing $C_{14}$TAB as a standard.

*2.1.3. Development of the film holder.* Historically, the first disjoining pressures were measured by Scheludko and Exerowa in 1959 with a so-called *Scheludko cell* [29] instead of the *porous-plate cell* shown in figure 2. In the original version, the film holder is simply a glass ring connected to a glass capillary and the film is made by sucking out liquid from the droplet formed in the glass ring. With the *Scheludko cell* the range of measurable disjoining pressures is limited to a few tens of pascals because of the low capillary entry pressure. Furthermore, the hole connecting the film to the bulk liquid in the capillary prevents an equal drainage of the film. With the *porous-plate cell* problems occur because of the high surface area of the porous disc. Strong adsorption has to be taken into account which contaminates the porous plate so it cannot be used for different systems. Furthermore, a large amount of solution (several tens of millilitres) is necessary to guarantee the saturation of the porous system with liquid.

A new approach for reducing the required amount of liquid is using the *bike-wheel cell* developed by Cascao Pereira *et al* [28]. In this cell an inner hole (0.75–1.5 mm diameter) holding the film (the hub) is connected radially by 24 small channels (the spokes) to an outer, larger size annulus (the wheel). The cell can be understood as a surface-reduced *porous-plate cell* combining the advantages of a *Scheludko cell* and those of a *porous-plate cell*:

(a) Due to the low surface area a smaller amount of sample is sufficient and the cell can be purified for re-use.
(b) The small diameter of the channels (16 $\mu$m) allows one to apply pressures up to $10^4$ Pa, close to what is obtained with the *porous-plate cell* (up to $7 \times 10^4$ Pa [5]).

The *bike-wheel cell* is especially suited for the investigation of large-molecular-weight species such as polymers or proteins and it is expected to play an important role in the future for studying $\Pi(h)$ curves. The main disadvantage of this cell seems to be its lavish microfabrication based on photolithography.

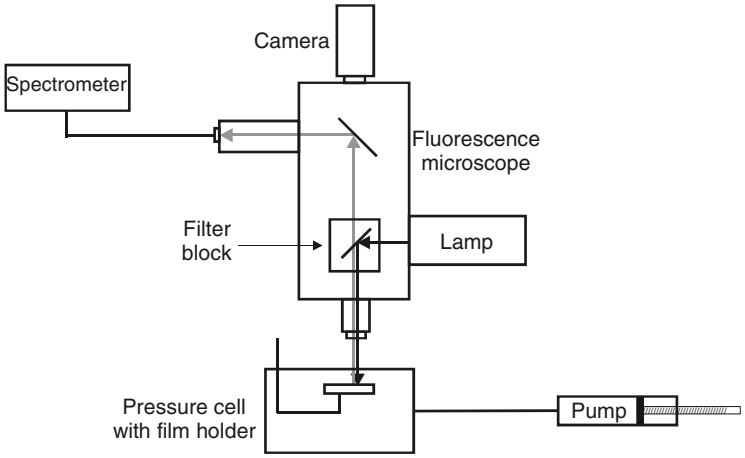


**Figure 3.** The experimental set-up of the *fluorescence TFPB*: a pressure cell, including the film holder, combined with a fluorescence microscope, a CCD camera, and a multichannel spectrometer. Redrawn with permission from *Macromolecules* [30].

*2.1.4. Fluorescence measurements on free-standing films.* To follow the expulsion of molecules with increasing outer pressure, dye molecules are entrapped in the film, and the films are investigated with a common TFPB combined with fluorescence techniques. The dye molecules can be either a probe [20] or a label covalently bound to a macromolecule [30]. The set-up of a *fluorescence TFPB* as used in [30] is shown in figure 3. It is a TFPB (see section 2.1.1), combined with a fluorescence microscope and a spectrometer. The fluorescence microscope is equipped with a filter block for the dye excitation (interference filter, dichroitic mirror, and a band-pass filter for emission). A further block provides the alternative possibility of observing the film with white light. The fluorescence images are captured by a high-resolution CCD camera. Alternately, the fluorescence signal can be analysed by a multichannel spectrometer coupled to the microscope. To avoid a superposition between the fluorescence signal and the reflected intensity, which is used for the interferometric determination of the thickness, the wavelength used for the thickness analysis should be separated from the excitation and the emission wavelength of the dye.

### *2.2. Emulsion films*

Replacing the gaseous phase in foam films by an oil phase, one creates an emulsion film. In addition, two different 'arrangements' of the liquids are possible, so one has to distinguish between oil/water/oil and water/oil/water emulsion films. From the physical point of view the determination of disjoining pressures and/or forces in these films is the same as for foam films. However, a lot of technical problems occur so, in addition to the modification of the TFPB, different techniques have been developed. The advantages and disadvantages of the most promising techniques will be discussed in the following.

*2.2.1. Oil/water/oil films.* Aveyard *et al* constructed a *liquid surface force apparatus*, LSFA, to measure $\Pi(h)$ curves of oil/water/oil emulsion films [31, 32]. Films down to 5 nm thickness are investigated in a pressure range from 50 to 2000 Pa. The radius of the films is only a few micrometres. The principle is to press an oil drop, which is attached to a flexible capillary, up to a macroscopic water/oil interface. The capillary is connected to a manometer containing the

same oil. The radius of the oil drop is controlled by the balance of the Laplace pressure inside the drop and the applied pressure. When the oil drop is moved up to the water/oil interface a thin water film is formed between the apex of the drop and the macroscopic interface. With this set-up both the force and the disjoining pressure can be measured. The force exerted on the oil drop as it is pressed up to the oil/water interface is determined from the deflection of the capillary whereas the disjoining pressure is given by the hydrostatic pressure applied to the oil in the capillary. The corresponding film thickness is derived by optical interferometry.

A novel approach for studying forces in oil/water/oil films is to measure the flocculation transition of oil-in-water emulsions [33, 34]. For this purpose sharp and reversible transitions between a flocculated and a non-flocculated state are induced, measured, and modelled in terms of surface forces. From the flocculation transition the critical disjoining pressure at which the film ruptures can be calculated. The technique is a promising tool for correlating the stability of macroscopic emulsions with the disjoining pressure acting within the thin liquid emulsion films. However, as only one characteristic point on the $\Pi(h)$ curve is measured, this technique does not replace but merely complements the above-mentioned LSFA.

A completely different way to investigate oil/water/oil emulsion films is the *magnetic chaining technique*, MCT, where forces instead of pressures are measured [35–38]. With this technique, force versus distance curves of monodisperse submicron-sized emulsion drops are obtained. The oil drops consist of a ferrofluid, which is a dispersion of iron oxide ($\gamma$-$Fe_2O_3$) particles in oil. The diameter of the $\gamma$-$Fe_2O_3$ particles is around 10 nm, whereas the oil drops are about 0.2 $\mu$m in diameter. In the absence of an external magnetic field these emulsions are non-magnetic since the magnetic particles in the oil drops are randomly oriented. However, an external magnetic field induces an attractive dipole force which can be controlled by the strength of the applied field. Since the magnetic field induces the formation of ordered chains, light is Bragg scattered, enabling the distance between two drops to be measured. The attractive dipole force balances exactly the repulsive force between the drops. As the former can be calculated exactly from the strength of the magnetic field and the distance of the drops, the deduced repulsive force can be plotted as a function of the distance leading to a well-known force–distance curve.

Last but not least, the *porous-plate technique* was modified by Dimitrova *et al* [39] to measure $\Pi(h)$ curves of oil/water/oil emulsion films. The experimental set-up explained in section 2.1 cannot be used because of the following two technical difficulties. First, to calculate the disjoining pressure the gas pressure $P_g$ in equation (1) has to be replaced by the oil pressure $P_{oil}$ of the oil phase surrounding the aqueous film. However, the needed pressure difference $\Delta P = P_{oil} - P_r$ cannot be measured because the pressure transducers are not resistant to organic liquids. Second, liquids are incompressible, so the pressure applied to the film cannot be set and controlled as easily as for the foam film. In the modified version of Dimitrova *et al* [39] the film is formed in a *porous-plate cell* by sucking liquid out of it. In contrast to the original version it is now the film holder itself that is directly connected to the pressure transducer. The transducer measures the difference between the pressure $P$ that is needed to suck out the liquid and the reference (atmospheric) pressure. Like in the original version the maximum attainable pressure is determined by the porosity of the disc, i.e. pressures up to several tens of kilopascals can be applied. Note that in the original version an excess pressure is applied to squeeze out the liquid of the film, whereas in the modified version the liquid is sucked out, i.e. that $\Delta P = P - P_r$ is negative for $P < P_r$. A great advantage of this set-up is the fact that it can be used for the investigation of both foam and emulsion films.

As the disjoining pressure can be converted to a force, disjoining pressure measurements can be compared with direct force measurements. Such a comparison is very important to show the reliability of each technique, as up to now we do not have an exact calibration

method for surface force techniques. Indeed, very similar results were obtained with the modified TFPB and the MCT technique [39]. Although in this review only techniques applicable to liquid interfaces are considered, we would like to mention that a comparison with forces measured between solid surfaces should be handled with care as completely different results are possible [6, 39, 40]. To sum up, one can say that none of the above-mentioned techniques simulate very well the conditions in a real emulsion film, which is formed when two micrometre-sized emulsion drops approach each other. The capillary pressure in these films is above several thousand pascals and the film radii are some micrometres. With the LSFA these small radii are realized but the pressure range is limited to 2000 Pa. The situation is opposite for the modified TFPB where high pressures can be applied but radii of more than 100 $\mu$m are usually considered. The drainage of these large films leads to the formation of 'dimples', an effect not seen for the smaller films in the LSFA. Last but not least, in the somewhat different MCT, ferrofluids are used and the question has to be clarified of how the addition of ferromagnetic particles to the oil phase changes the overall behaviour of the system. Keeping these points in mind, one can conclude that it is only the combination of the above-mentioned methods that will allow us to simulate real colloidal systems more accurately.

*2.2.2. Water/oil/water films.* So far, not much work has been done on the disjoining pressure of non-aqueous emulsion films. This is rather astonishing as the stability of water-in-oil emulsions is very important not only for the general understanding of colloidal stability but also for particular applications, for example in the oil industry [24], or for the specific treatments of nuclear wastes [41]. Neither the LSFA nor the MCT technique mentioned above have been adapted to water/oil/water films. To our knowledge, the first disjoining pressure study of oil films, which were stabilized by a polymer, was performed by Anklam *et al* [42]. In this very interesting study a thin-film apparatus is used which allows the application of an electric field across the film and its interferometric observation. When a voltage is imposed across the film, a compressional force per unit area is produced. As the compression force increases, the disjoining pressure in the film grows to balance the forces on the film interfaces. The thickness of the oil film can be determined by measuring the film capacitance and the film area. Note that only the film area and not the film thickness is determined interferometrically. Thus, $\Pi(h)$ curves are obtained using an electric field to compress the film and measuring the thickness. Two drawbacks have to be mentioned. First, the compressive force, and thus the disjoining pressure, is a function of the applied voltage and the film thickness (see equation (2) in [42]). As a consequence, the compressive force range is very small for thick films. Second, only 'pseudo-disjoining pressures' are obtained. The electrical compressive force has to be corrected by the capillary pressure, which is not known. However, this correction is in the range of 100 Pa, so it only plays a role at low compressive forces.

Not surprisingly, the *porous-plate technique* has also been modified to investigate the 'inverse' films. Drainage times and equivalent film thicknesses [24a] as well as disjoining pressure curves [24b] of diluted bitumen films have been reported. In the first disjoining pressure study on oil films performed with the TFPB, $\Pi(h)$ curves of dodecane films stabilized by different surface-active agents were measured [41]. As for the oil/water/oil films, the film thickness is changed by sucking out the liquid of the film. Moreover, because of the density difference between oil and water, care must be taken to avoid a creaming of the oil film and a sedimentation of the water film. For this purpose, the hole has to be as small as possible. In [24] and [41] a hole diameter of about 750 $\mu$m is used instead of the usual 1–2 mm. However, an additional problem occurs, when water/oil/water films are investigated with the *porous-plate technique*. As the porous disc consists of sintered glass, i.e. is not wetted by oil, it has to be hydrophobized. This was done by simply soaking the film holder in the respective oil phase

for a minimum of 24 h and cleaning it afterwards with ethanol and toluene [24]. A more elaborate technique is to silanize the porous plate via the gas phase, a procedure that is well known to hydrophobize glass surfaces (see for example the preparation of the MASIF surfaces in [43]) and that was now adapted to the *porous-plate cell* [41]. The set-up in [41] is tested with the same system as was used in [42]. The fact that such complex systems (Saint-Jalmes *et al* report that the comb copolymer used to stabilize the film is not characterized adequately) were used to calibrate new set-ups underlines the need for calibration standards not only for the foam but also for the emulsion films.

### *2.3. Pseudo-emulsion films*

While the papers dealing with the disjoining pressure in emulsion films are few compared to those dealing with $\Pi$ in foam films, papers about the disjoining pressure in pseudo-emulsion films are even rarer. Pseudo-emulsion films are asymmetric oil/water/air films which are of interest as any mechanism of foam destruction by emulsified oil includes the formation and rupture of these films. Two different techniques have been developed with which the disjoining pressure of pseudo-emulsion films is measured. One of them is called the *film trapping technique*, FTT [44–46]. With this technique the entry barrier, which prevents the emergence of pre-emulsified oil drops on the water/air interface, can be measured. For that purpose, oil drops in a surfactant solution are entrapped between a glass substrate and air. By increasing the air pressure the oil drops are compressed until—at a given critical capillary pressure—the asymmetric film formed between the oil drop and the solution surface ruptures. This rupture point is the moment where the drop enters the water/air surface and the corresponding critical pressure $P_C^{CR}$ is referred to as the *barrier to drop entry*. In the case of planar films, $P_C^{CR}$ equals $\Pi_{AS}^{CR}$, i.e. the critical disjoining pressure at which the film ruptures. However, for curved films neither $\Pi_{AS}^{CR}$ nor a $\Pi_{AS}(h)$ curve can be calculated exactly from the experimental data as the film curvature depends on the drop deformation, which in turn is determined by the applied capillary pressure $P_C$. Thus these values can only be estimated by an iterative procedure [45]. An outstanding advantage of the FTT is that large, strongly curved films can be investigated simulating real pseudo-emulsion films better than the small, planar films investigated with the *porous-plate technique* (see below). Thus, the FTT is an important complement to the classical method and will surely attract a lot of attention with respect to the 'disjoining pressure discussion' going on.

Again, it is the *porous-plate technique* with which $\Pi(h)$ curves of planar asymmetric films can be measured directly [47, 48]. The main challenge is the construction of the appropriate film holder. Plane-parallel films are required for the measurements, i.e. the pressures on the gas and the oil side of the film have to be equal. This criterion leads to the following relation: $P_c = 2\sigma_{wg}/R_{wg} = 2\sigma_{ow}/R_{ow}$ where $\sigma_{ij}$ is the tension between the phases $i$ and $j$, namely water (w), gas (g), and oil (o), and $R_{ij}$ the radius of curvature at the corresponding interface. Consequently, the differences in $\sigma_{ij}$ have to be compensated by $R_{ij}$. A shortcoming of the technique is the time-consuming feature that the exact hole geometry can only be determined by trial and error (see [48] for details). However, to our knowledge, up to now this technique is the only suited for determining $\Pi(h)$ curves of pseudo-emulsion films.

To sum up, one can say that the intensive work on improvements and the interest in adapting the principle of the 'original' TFPB to emulsion and pseudo-emulsion films underlines the potential of this method. We believe that this technique will increase in importance, as it seems to be the only technique that can be adapted to all kinds of thin liquid films. The aim is to have a general set-up with which all above-mentioned films can be investigated over a large range of disjoining pressures and film radii. Of course, the development and use of the other

techniques is equally important, as they provide perfect complements and alternatives to the classical *porous-plate technique*.

## 3. Ionic versus non-ionic surfactants

In section 3, disjoining pressure versus thickness curves, i.e. $\Pi(h)$ curves, of non-ionic (section 3.2) and ionic (section 3.3) surfactant foam and emulsion films will be compared. Additionally, first results on the influence of additives and impurities on the $\Pi(h)$ curves of the corresponding pure surfactant solutions will be discussed. Sections 3.2 and 3.3 are restricted to thin liquid emulsion and foam films stabilized by low-molecular-mass surfactants. Results obtained for pseudo-emulsion films (see section 2) and for films stabilized by polymers (see section 4) are left out. In order to explain the significant differences between non-ionic and ionic surfactant films the origin of the surface charges will be reviewed in section 3.1.

In the introduction it has already been mentioned that the electrostatic and the steric repulsion between the interfaces are decisive factors for the stabilization of a CFB and a NBF, respectively. Usually, the CBF is analysed in terms of the DLVO theory [49] from which the surface potentials $\psi_0$ can be extracted. The corresponding surface charge densities $q_0$ can be calculated by using the Grahame equation [49]

$$q_0 = \sqrt{8\varepsilon\varepsilon_0 RTc}\,\sinh\left(\frac{F\psi_0}{2RT}\right). \tag{4}$$

However, the application of the DLVO concept to thin liquid films is limited, as the film surfaces have both spatial and surfactant density fluctuations, which is not considered in the classical DLVO theory. A semi-quantitative treatment of these fluctuations is presented by Bergeron [1, 12]. As for the CBF, the forces that stabilize the NBF are not completely understood, so a quantitative analysis of the entropic confinement forces acting in a NBF [2] is not yet possible. It is important to realize that not all surfactant solutions support both types of film. Some surfactant solutions have a CBF region that ruptures at high pressures without forming a NBF, whereas others stabilize only NBFs. How the formation of a CBF and/or a NBF is determined by the type of surfactant, the surfactant concentration, the electrolyte concentration, and the pH will be focused on in sections 3.2 and 3.3. In addition, the influence of surface-active additives and impurities on the type of film formed will be discussed. As we need to know the origin of the surface charges in order to understand the influence of the above-mentioned parameters on the $\Pi(h)$ curves, the current discussion is reviewed in the following section.

### *3.1. Origin of the charges at water/air and water/oil interfaces*

Considering thin liquid films stabilized by surfactants, one at first expects negatively charged surfaces for anionic, positively charged surfaces for cationic, and non-charged surfaces for non-ionic surfactants. The surfaces of ionic surfactant films do indeed have the same charge as the surfactant. However, in the presence of cationic surfactants, a charge reversal from negative to positive is observed with increasing concentration at very low surfactant concentrations [50]. Furthermore, thin liquid films of non-ionic surfactants are also stabilized by electrostatic double-layer forces (see section 3.2), which means that surface charges must be present. The sign of the net charge was obtained from measurements of the zeta potential, which led to the result that the water/air [51, 52] as well as the water/oil interface [53, 54] are negatively charged in the presence of non-ionic surfactants. Addition of anionic surfactants changes the zeta potential in the expected way, namely increases the negative potential, whereas a cationic

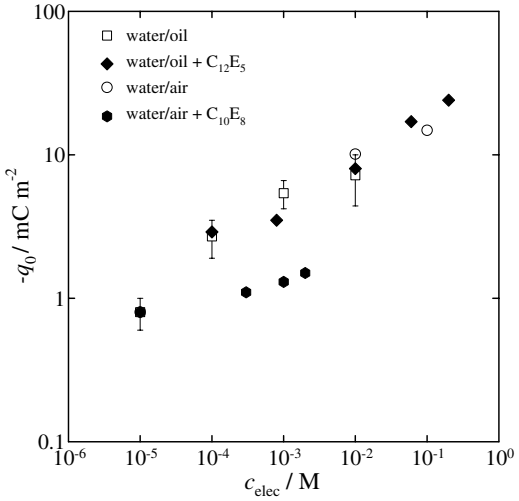


**Figure 4.** Surface charge densities $q_0$ as a function of the electrolyte concentration for four different systems: (□) bare water/oil interface, pH = 6 [54]; (○) bare water/air interface, pH = 6 [55]; (♦) $C_{12}E_5$-loaded water/oil interface, pH = 5.5, $c(C_{12}E_5) = 2 \times 10^{-5}$ M (1/3 cmc) [32]; (⬢) $C_{10}E_8$-loaded water/air interface, pH = 5.5, $c(C_{10}E_8) = 8 \times 10^{-4}$ M (2/3 cmc) [14]. In [54, 55] the electrophoretic mobility but in [14, 32] $\Pi(h)$ curves were measured to obtain $q_0$. Note that at $c_{elec} = 10^{-5}$ M the same charge is obtained for water/air, water/oil, and water/air + $C_{10}E_8$.

surfactant causes a charge reversal from negatively to positively charged interfaces [34, 53]. Discussing the origin of the charge in the presence of non-ionic surfactants, one has to be aware of the fact that the water/oil (see [54], and references therein) as well as the water/air interface [52, 55, 56] are negatively charged even in the absence of any surfactant. Furthermore, the charge at the bare water/air interface is high enough to stabilize aqueous films without any surfactant as shown in a unique experiment by Exerowa *et al* [57]. The discussion of the origin of the negative charges is mainly based on the following four arguments [13, 14, 23, 54, 57, 58].

(a) *Adsorption of amphiphilic anionic impurities*: The adsorption of amphiphilic anionic impurities as the source of the negative charge cannot be entirely rejected but it is highly unlikely as a lot of experimental precautions were taken to avoid contaminations [54]. Furthermore, the reproducibility of the results obtained with different equipment and surfactants (see section 3.2) can hardly be explained with impurities. Note that the amount of charge at the bare interfaces is equal or even higher than in the presence of non-ionic surfactant (see figure 4). Thus, amphiphilic ionic impurities can be ruled out as sources for the negative charge—at least for the bare interfaces. Only recently, the influence of impurities has been investigated in detail. The $\Pi(h)$ curves of an 'as-received' and the corresponding 'surface chemical pure' sample were compared [10]. The 'as-received' sample was indeed contaminated with traces of ionic surfactant. However, the absence of these traces did not lead to uncharged but solely to slightly less charged surfaces. Thus surface-active ionic impurities alter the amount of charge but they are not its source.

(b) *Specific adsorption of $HCO_3^-$ ions*: Due to dissolved $CO_2$ from air, negatively charged $HCO_3^-$ and $CO_3^{2-}$ are present in the aqueous solution. The hypothesis that the surface charge may be created by the specific adsorption of these ions was discarded only recently. Marinova *et al* [54] performed two measurements at equal pH and electrolyte concentration $c_{elec}$, i.e. equal ionic strength, in the absence of surfactant. In one case they adjusted the

pH and $c_{elec}$ by adding $Na_2CO_3$, and in the other case the pH and $c_{elec}$ were adjusted by adding NaCl and NaOH. The experiments showed that the zeta potentials at the bare water/oil interface were equal, so a specific adsorption of $HCO_3^-$ and/or $CO_3^{2-}$ ions can be ruled out. Furthermore, non-ionic surfactant foam films were investigated under air and under a nitrogen atmosphere [58]. The evaluation of the $\Pi(h)$ curves led to the same surface potentials, which underlines that the specific adsorption of $HCO_3^-$ and/or $CO_3^{2-}$ is not the source for the negative surface charge.

(c) *Specific adsorption of negatively charged electrolyte ions*: Zeta and surface potential measurements are usually performed in the presence of electrolyte to work under known electrostatic conditions. Thus the specific adsorption of negatively charged electrolyte ions was discussed as a possible origin of the interfacial charges. This argument is underlined by theoretical studies of the interface between an electrolyte solution and air, which have been presented only recently [59]. According to the authors, the calculations demonstrate that the heavier halogen anions have a propensity for the interface that is proportional to their polarizability. However, three experimental observations make this argument unlikely. First, for non-ionic surfactant foam films, equal $\Pi(h)$ curves were measured in the presence of KCl and $KClO_3$ at equal ionic strength [58]. Note that chloride ions desorb from the interface, whereas chlorate ions adsorb. Therefore, if the electrolyte determined the interfacial charge in thin liquid films, the corresponding $\Pi(h)$ curves would be significantly different. Second, at constant electrolyte concentration the interfacial charge depends on the pH for both the bare [23, 54, 55] and the surfactant-loaded [13, 14, 23, 60] interfaces. Third, the isoelectric point, i.e. the point where the amount of positively and negatively charged ions is equal with the result that the surface charge is zero, does not depend on the salt concentration. This holds for the bare water/air interface [55] as well as for non-ionic surfactant foam films [61]. In conclusion, even if negatively charged electrolyte ions contribute to the surface charge, they are not the charge-determining ions.

(d) *Specific adsorption of $OH^-$ ions*: The most favoured explanation of the negatively charged interfaces is a specific adsorption of $OH^-$ ions. However, in the presence of non-ionic surfactants the $OH^-$ ions are not simply attached to the head-group as was assumed some years ago [62, 63]. If that were the case, the amount of charge would increase with increasing surfactant concentration; however, the contrary is observed. Thus the $OH^-$ ions must be adsorbed directly at the water/air and the water/oil interface, respectively. In other words, the charge is a property of the bare interfaces, and the surfactant only modifies its value. A negative water/air interface is in absolute agreement with the observation that the surface charge is negative not only in the presence of non-ionic surfactant, but also in the presence of small amounts of cationic surfactant. The negative charge has to be compensated before the surface can become positive. The questions that remain are: Where do the $OH^-$ ions come from? How many charges are needed for the measured electrical potentials? What is the driving force for a specific adsorption? What does the adsorption look like on a molecular scale? The first two questions are easy to answer. The $OH^-$ ions come from the dissociation of water and the amount of charges can be calculated from the measured zeta and surface potentials. Such a calculation yields a maximum adsorption density for the $OH^-$ ions of $10^{-8}$–$10^{-7}$ mol $m^{-2}$ at a pH of about 8 [14, 54]. On condition that the adsorption layer has a thickness of 1–10 nm, the corresponding $OH^-$ concentration has to be $10^{-1}$–$10^{-3}$ M, whereas the $OH^-$ bulk concentration at pH = 8 is only $10^{-6}$ M. Although the charge density is extremely low (about 70 $nm^2$/charge), a specific adsorption process is needed to explain such a concentration gradient. The present discussion is based on the fact that the water molecules at the water/air and water/oil

interface are ordered [49, 64]. Strong hydrogen bonds between the interfacial water and $OH^-$ ions could lead to the specific adsorption of $OH^-$ ions. Although these bonds also exist in the bulk water, it is proposed by Marinova *et al* that fractions of the H bonds in the bulk are broken due to the Brownian motion. In other words, specific adsorption could result from restrictions in the movement of the water molecules in the interfacial layer leading to more pronounced H bonds between $OH^-$ and water molecules [54]. The adsorption mechanism itself is far from being clear. To sum up, one can say that a qualitative explanation of the origin of the charges can be given and that the focus of research work in this field is, and will be, on its quantitative explanation. The effect of surface charges on thin liquid films will be discussed in the following two sections.

### *3.2. Films stabilized by non-ionic surfactants*

Although the electrostatic stabilization of foam films containing non-ionic surfactants is a well-known phenomenon, only few papers deal with $\Pi(h)$ curves of non-ionic surfactants [9–11, 13, 14, 19, 32, 61, 63]. The focus is on four particular surfactants: the alkyl polyglycolethers $C_{10}E_4$ [14, 63] and $C_{10}E_8$ [14] and the two sugar surfactants octyl glucoside $C_8G_1$ [9, 13, 19] and dodecyl maltoside $C_{12}G_2$ [11]. In addition, Binks *et al* [32] measured $\Pi(h)$ curves of oil–water–oil emulsion films stabilized by $\beta$-$C_{10}G_1$ and $C_{12}E_5$, respectively, with a LSFA (see section 2.2). The interpretation of the results by means of the DLVO theory leads to the charge density at the interface, which will be focused on in the following.

In figures 4–6, surface charge densities $q_0$ of bare and surfactant-loaded interfaces are shown as a function of the electrolyte concentration, the surfactant concentration, and the pH. Some representative error bars are shown. Additional data can be found in [23]. Note that in [54, 55] the electrophoretic mobility, in [60] the equilibrium film thickness, and in [11, 13, 14, 32] the complete $\Pi(h)$ curves were measured to obtain the surface charge densities. As some of the references quoted present the zeta or surface potentials instead of $q_0$, we calculated the corresponding $q_0$ according to equation (4) [54] in order to compare the results. As shown in figure 4, the surface charge density increases with increasing electrolyte concentration. The data for the bare interfaces agree perfectly well, i.e. the charges of the water/air and the water/oil interfaces are very similar in sign and magnitude. Though measured at a slightly different pH, the results for the surfactant-loaded water/oil interface do not differ from those for the bare interfaces. In other words, the adsorption of non-ionic surfactant does not change the surface charge. However, this statement only holds for low surfactant concentrations, as can be seen in figure 4. Whereas no influence is seen for a concentration of 1/3 cmc, significantly lower charges are measured at a concentration of 2/3 cmc. The resulting dependence of the surface charge density on the surfactant concentration is shown in more detail in figure 5. As already deduced from figure 4, it is seen that $q_0$ decreases with increasing surfactant concentration. Note that it is not the absolute concentration that is of importance but the surface concentration, which is directly correlated to the cmc (at the cmc the surface concentration has reached its maximum). Although the error range of the data is still significant, it can be seen that the surfactant-loaded water/oil and the water/air interfaces behave similarly, in accordance with the results for the bare interfaces. The lower $q_0$-values obtained for the sugar surfactants $\beta$-$C_8G_1$ and $\beta$-$C_{12}G_2$ are mainly due to the lower salt concentration of the corresponding solution. Last but not least, pH-dependent measurements are shown in figure 6. The differences in absolute values reflect the different measuring conditions—high electrolyte concentrations lead to high surface charge densities $q_0$ (open circles, [55]), whereas high surfactant concentrations result in low $q_0$ (filled triangles, [14]). However, it is quite obvious that $q_0$ increases with increasing pH. To sum up, one can say that the bare as

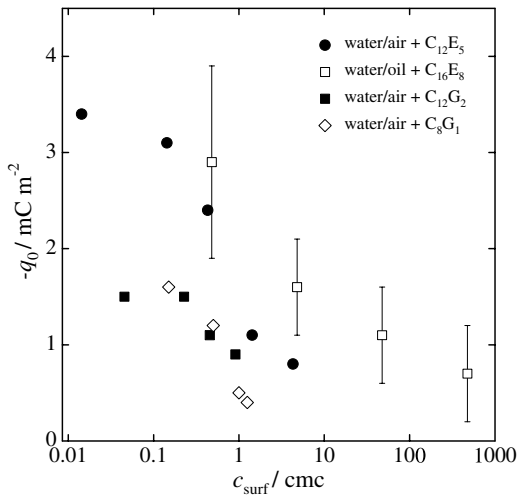


**Figure 5.** Surface charge densities $q_0$ as a function of the surfactant concentration for four different systems: (●) $C_{12}E_5$-loaded water/air interface, pH = 5.7, $c$(KCl) = $10^{-3}$ M [60]; (□) $C_{16}E_8$-loaded water/oil interface, pH = 6, $c$(NaCl) = $10^{-3}$ M [54]; (■) $C_{12}G_2$-loaded water/air interface, pH = 5.7, $c$(NaCl) = $10^{-4}$ M [11]; (◇) $C_8G_1$-loaded water/air interface, pH = 5.7, $c$(KBr) = $10^{-4}$ M [13]. In [54] the electrophoretic mobility, in [60] equilibrium film thicknesses, and in [11, 13] the complete $\Pi(h)$ curves were measured to obtain $q_0$.

well as the surfactant-loaded water/air and water/oil interfaces are negatively charged. The surface charge density $q_0$ (a) increases with increasing electrolyte concentration, (b) decreases with increasing surfactant (non-ionic) concentration, and (c) increases with increasing pH. These observations will be discussed in the light of the specific adsorption of $OH^-$ ions at the water/air and the water/oil interfaces, respectively, presented in section 3.1.

(a) The increase of the surface charge with increasing electrolyte concentration is accompanied by a decrease of the surface potential [11, 58]. According to the Boltzmann distribution, the concentration of ions between two charged surfaces is

$$c_{ion}^0 = c_{ion}^\infty \exp\left(\frac{F\psi_0}{RT}\right) \tag{5}$$

where $c_{ion}^0$ and $c_{ion}^\infty$ are the ion concentration at the interface and in the bulk far away from the interface, respectively. $F$ is the Faraday constant. Consequently, as the negative potential $\psi_0$ decreases in magnitude, $c_{ion}^0$ increases resulting in an increase of the surface charge. (Note that the significant changes in the film thickness, which are observed with increasing electrolyte concentration, are not due to the small changes in $\psi_0$ but rather to the much more pronounced decrease of the Debye length.) Because equation (5) also holds for $OH^-$ ions, it agrees with the idea of specific $OH^-$ adsorption. However, this argument does not exclude any other ion as the origin of the charges. Note that equation (5) does not depend on any adsorption mechanism for the ions.

(b) The decrease of the surface charge with increasing surfactant concentration is shown in figure 5. The explanation commonly given is a decrease of the area available for the adsorption of $OH^-$ ions. The ions are expelled from the interface while a (non-ionic) surfactant adsorption layer is built up. However, there is ample space for $OH^-$ ions even at very high adsorption levels (i.e. next to the cmc), so the expulsion of the ions is not for want of geometrical space. Remembering the fact that the water molecules at

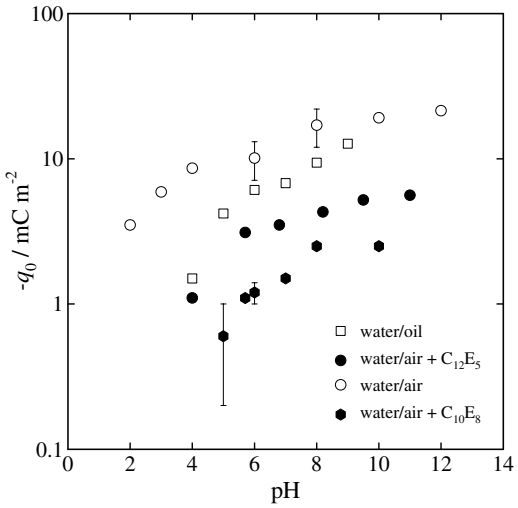


**Figure 6.** Surface charge densities $q_0$ as a function of the pH for four different systems: (□) bare water/oil interface, $c$(NaCl) $= 10^{-3}$ M [54]; (○) bare water/air interface, $c$(NaCl) $= 10^{-2}$ M [55]; (●) $C_{12}E_5$-loaded water/air interface, $c(C_{12}E_5) = 10^{-5}$ M (1/7 cmc), $c$(KCl) $= 10^{-3}$ M [60]; (⬢) $C_{10}E_8$-loaded water/air interface, $c(C_{10}E_8) = 8 \times 10^{-4}$ M (2/3 cmc), $c$(KCl) $= 3 \times 10^{-4}$ M [14]. In [54, 55] the electrophoretic mobility, in [60] equilibrium film thicknesses, and in [14] the complete $\Pi(h)$ curves were measured to obtain $q_0$.

the water/air and water/oil interface are highly ordered (see section 3.1), one can argue that in the presence of surfactant the interfacial water consists mainly of hydration water attached to the polar head-groups. The more surfactant is adsorbed, the fewer 'oriented' water molecules there are present, which was the condition for specific $OH^-$ adsorption. In this case, a decrease of the interfacial charge with increasing surfactant concentration is expected. However, it was found that the charge is nearly constant at low surfactant concentrations and does not decrease significantly until the concentration approaches and exceeds the cmc [11, 58, 60]. This behaviour contrasts sharply with the adsorption of the surfactant, which changes significantly at low concentrations and already stays constant far below the cmc. Thus, a typical competitive adsorption between surfactant and hydroxide does not take place; otherwise the change in surface charge densities would be parallel to the change in surfactant adsorption. A qualitative explanation of this observation is a change of state in the surfactant adsorption layer near its saturation by which the adsorption of the $OH^-$ ions is deranged [60]. An attempt at a quantitative description is the two-site mechanism proposed by Karraker *et al* [14]. The idea is that there are adsorption sites on the interface at which only surfactant can adsorb ($S_1$), whereas at other sites either surfactant or hydroxide can adsorb ($S_2$). Note that the surfactant adsorption (0.5–0.4 nm$^2$/surfactant) is two orders of magnitude larger than the hydroxide adsorption (around 100–500 nm$^2$/charge), which indicates a 'permanent surfactant background' ($S_1$). It is only for the $S_2$ sites that competition occurs. Although this model does not describe all experimental results quantitatively, it is a first step towards describing the molecular mechanism behind the decrease of $q_0$ with increasing surfactant concentration.

(c) The assumption that the electrostatic repulsion in non-ionic foam films is due to the specific adsorption of hydroxide ions at the water/air interface is confirmed by pH-dependent measurements (see figure 6). It was shown [13, 14, 60, 61] that at constant ionic strength a decrease of the pH of the solution leads to a decrease in the surface charge density until

it disappears at a certain pH value. At this particular point, which is called the isoelectric point pH* [57], all CBFs are unstable, i.e. the film ruptures or a NBF is formed depending on the surfactant concentration [60]. A detailed discussion of the isoelectric point can be found in [23] (section 3.3.2) and in [11]. To sum up, one can say that the surface charge density increases with increasing pH as the overall amount of $OH^-$ ions increases. However, a maximum coverage of $OH^-$ ions is reached at very low charge densities (around 2.5 mC $m^{-2}$ corresponding to 65 $nm^2$/charge [14]), underlining the argument that the adsorption is not limited by finite size but by the availability of adsorption sites.

Knowing how the pH, the electrolyte, and the surfactant concentration influence the interfacial charge of thin liquid films, we can now address the question of how the charge influences the stability of the corresponding films. Generally speaking, a decrease in $q_0$ leads to a destabilization of the CBF until it is completely unstable at low $q_0$. If the destabilization of the CBF is accompanied by the stabilization of a NBF (see below), the film is not unstable at low surface charge densities, but immediately forms a sterically stabilized NBF. As the NBF formation requires a very high surfactant coverage at the surface, the CBF–NBF transition is only expected at surfactant concentrations near to the cmc.

In this connection it has to be underlined that the stability of thin liquid films is not solely determined by the surface charge but also by the concentration and the structure of the surfactant. In other words, similar surface forces do not automatically result in similar film stabilities. The influence of the surfactant concentration on the stability of the film is shown by the concentration-dependent $\Pi(h)$ curves of $\beta$-$C_8G_1$ [13] and $C_{10}E_4$ [65]. For example, films of a 3 mM (1/7 cmc) $\beta$-$C_8G_1$ solution are difficult to obtain, whereas those of a 10 mM (1/2 cmc) $\beta$-$C_8G_1$ solution are stable up to 3000 Pa although the charge decreases from 1.6 for the 3 mM solution to 1.2 mC $m^{-2}$ for the 10 mM solution. Thus, an increase of the surfactant concentration (see figure 5) results in both a decrease of the interfacial charge and an increase of the stability. The former effect destabilizes the CBF, whereas the latter is stabilizing. With regard to the surfactant structure, it has been shown by Karraker *et al* [14, 58] that the structure of the surfactant has little influence on the magnitude of the long-range forces, whereas it dictates the stability of the film as well as its ability to form a NBF. For example, a surface charge of around 1.5 mC $m^{-2}$ is not enough to stabilize a $\beta$-$C_8G_1$ film [13], whereas it is sufficient for obtaining very stable $\beta$-$C_{12}G_2$ films [11]. Generally speaking, the stability of the film is based on the surface elasticity of the interface. It was shown for the cationic alkyltrimethylammonium bromides $C_n$TAB that at least a tetradecyl chain, i.e. $n = 14$, is required to stabilize a film (see section 3.3, [12]). For the non-ionic alkyl tetraethylenglycolethers $C_nE_4$, $n$ has to be $\geqslant$10 to obtain stable films [58], whereas for the sugar surfactants a hydrophobic octyl chain is sufficient for the formation of thin liquid films [13]. However, in all cases the elasticity of the surface increases with increasing length of the hydrophobic chain. Usually the stability of thin liquid films is discussed in terms of Gibbs elasticities [10, 12, 13], which can be misleading. The Gibbs elasticity is the hypothetical elasticity of a two-dimensional surface at infinitely high frequencies without any contact to the bulk phase. However, the elasticity of real surfaces depends strongly on the concentration of the bulk phase and on the frequency of the disturbance. For example, the Gibbs elasticities $\varepsilon_0^\sigma$ increase with increasing concentration, whereas measurements at finite frequencies lead to a maximum of the elasticity at intermediate concentrations [68]. Reliable rheological parameters of fluid surfaces which could clarify and quantify this point are still quite few in number [66–71]. Last but not least it has to be mentioned that the stability of a NBF requires not only high elastic interfaces but also large head-groups. For example, stable CBFs are formed by the surfactants $C_{10}E_2$, $C_{10}E_4$, and $C_{10}E_8$, whereas only $C_{10}E_8$ and $C_{10}E_4$ are able to build a NBF [58].

Considering the limited number of complete $\Pi(h)$ curves published so far, it is not astonishing that the influence of surface-active additives and impurities on the film stability and the type of film formed has not been investigated systematically. Although Persson *et al* [10] investigated the influence of surface-active impurities on the surface properties of $\beta$-$C_{10}G_2$ the impurity itself was not characterized. In order to understand the influence of additives, studies under defined conditions are needed, which means that both the kind and the amount of additive must be known. The influence of additives is of great technical relevance as commercial products are based on mixtures. The interplay of the different surface-active components in the formulation is expected to play the major role as regards film and foam stability. To our knowledge, up to now only two studies have been published in which the influence of a long-chain alcohol on the stability of ionic foam films was investigated [12, 72]. In both cases the alcohol stabilizes the film (see section 3.3). Contrary to these findings, first experiments with non-ionic foam films demonstrate that the addition of a long-chain alcohol is rather destabilizing [65]. In this work, the influence of decanol on the properties of $C_{10}E_4$ films is investigated at concentrations below and above the cmc. It was found that adding decanol to pure $C_{10}E_4$ solutions has only a minor effect on the CBF and no effect on the NBF. For the CBFs a small decrease of the surface charge and thus a slight decrease of the film stability were observed. The findings described so far allow us to speculate about the influence of impurities and/or additives. Additives that increase the surface elasticity stabilize the film. Whether a CBF or a NBF is stabilized depends on the charge of the additive. It is obvious that each additive has to be considered separately with regard to both its influence on the surface elasticity and the surface charge. In order to develop a structural concept for estimating the effect of additives, systematic experimental data are needed.

### *3.3. Films stabilized by ionic surfactants*

Comparing thin liquid films stabilized by ionic surfactants with those stabilized by non-ionics, one has to be aware of the fact that the origins of the surface charge are different. In the case of non-ionics the source of the charge is the specific adsorption of $OH^-$ ions (see sections 3.1 and 3.2), whereas for the ionics it is the surfactant itself that carries the charge. Consequently, differences between non-ionic and ionic surfactant films are observed. As each ionic surfactant carries a charge, $q_0$ increases with increasing surfactant concentration [32, 50, 73], whereas a decrease is observed for non-ionics (see figure 5). In contrast to the case for non-ionic surfactant films, no rupture or NBF formation but a stepwise thinning (see section 4) is observed at concentrations above the cmc. However, a CBF–NBF transition can be induced by adding salt (see below). Furthermore, the addition of electrolyte has different effects on the surface charge density $q_0$ as it changes the adsorption density of ionic surfactants, whereas the adsorption of non-ionics is usually not influenced. Last but not least, the subtle effect of the pH on disjoining pressure (see figure 6) cannot be observed for ionic surfactants, as the interfacial charge coming from the surfactant is much larger than the charge coming from adsorbed $OH^-$ ions. In the present section we will summarize the work on $\Pi(h)$ curves of ionic surfactant excluding studies of the stepwise thinning, which will be referred to in section 4. The studies published so far focus on the influence of the electrolyte concentration at a given surfactant concentration. Unfortunately, not much work has been done on the influence of the surfactant concentration on the disjoining pressure. In the following, measurements of the equilibrium thickness and of $\Pi(h)$ curves of different anionic and cationic surfactants will be discussed and compared.

Most thin liquid film studies deal with the anionic surfactant SDS. This is somewhat surprising, as it is known that the hydrolysis of SDS in aqueous solution leads to the formation

of surface-active dodecanol. Therefore, interpreting results for SDS one should be aware of the dramatic influence of dodecanol on the thickness [5] and the stability of ionic surfactant films [12]. At concentrations around the cmc a CBF of 20–12 nm thickness is found, which is stable to pressures greater than 70 kPa [3, 5, 16]. An increase of the ionic strength by the addition of salt leads to smaller thicknesses and to a steeper decay in accordance with the DLVO theory. Furthermore, the addition of salt could lead to the formation of a NBF. A detailed study of the influence of the electrolyte concentration on the CBF–NBF transition was published by Exerowa *et al* [74]. $\Pi(h)$ curves of a 0.001 M SDS solution were measured as a function of the NaCl concentration. It was found that for NaCl concentrations lower than 0.165 M the CBF ruptures in a defined pressure interval. The pressure of rupture increases with increasing salt concentration; i.e. the stability of the film increases. However, at NaCl concentrations higher than 0.165 M, a CBF–NBF transition occurs at a certain pressure. In contrast to the pressure of rupture, the pressure of transition decreases with increasing NaCl concentration, which indicates an increasing tendency for NBF formation. For example, for a 0.001 M SDS solution containing 0.18 M NaCl an abrupt transition in the thickness from 7 to 4.5 nm is observed at pressures as high as 90 kPa [3, 5, 74] whereas it is only 150 Pa in a 0.3 M NaCl solution [74]. (Note that non-ionic surfactants can form a NBF without adding salt or applying pressure!) These results can be understood if one realizes that the cmc of ionic surfactants decreases on adding salt. Thus at a constant surfactant concentration the adsorption at the water–air interface can be tuned by the salt concentration. The cmc of the 0.001 M SDS solution considered is reached at a NaCl concentration of 0.18 M. In other words, NaCl concentrations around 0.18 M are needed to obtain a CBF–NBF transition in a 0.001 M SDS solution as the NBF formation requires a densely packed surfactant film. The origin of the short-range forces stabilizing the NBF are still under discussion. Steric forces—as accepted for the non-ionic surfactants due to their large head-groups—are questionable as the head-groups of usual ionic surfactants are not very large. Thus the adsorption of highly hydrated counterions at the interface is assumed, which results in repulsive forces because a further approach of the interfaces would require dehydration of these ions [75, 76]. With respect to the forces stabilizing the CBF it has to be mentioned that the experimental results obtained for SDS cannot be interpreted in terms of the classical DLVO theory [74]. Sentenac *et al* [16] proposed a model with which the surface charge and the surface potential are not only regulated by electrostatic but also by hydrophobic forces. Although the theory describes accurately the $\Pi(h)$ curves of SDS in the presence of NaCl, the description of the corresponding CsCl curves is not satisfactory. According to the authors a modified theory including attractive dispersion forces may account for the experimental data. A completely different approach is the theory of enhanced colloidal interaction which describes the effect of interfacial forces on the adsorption density of the surfactant [77]. A change of the adsorption density at small distances not considered in the DLVO theory could probably explain the discrepancies between the experimental data and the theoretical DLVO curve. Work dealing with this question is under way [78].

Different results were obtained for negatively charged aerosol-OT (AOT) films in the presence of LiCl and CsCl, respectively [17]. Whereas the behaviour of the CsCl films can be described quite well by a classical DLVO approach, the presence of LiCl results in an additional repulsion up to separations of 10 nm. This phenomenon is interpreted as a long-range hydration effect. It is argued that the water molecules surrounding the counterions screen the net charge with the result that the net charge of the $Li^+$ counterions is smaller than that of the corresponding $Cs^+$ due to the larger number of hydrations. Thus, at equal ionic strength, the Debye length in the LiCl films is larger than in the CsCl films resulting in a shift of the $\Pi(h)$ curves towards higher thicknesses.

Black *et al* [79] measured $\Pi(h)$ curves of three different anionic surfactants, namely sodium *p*-(3-dodecyl)benzene sulfonate ($3C_{12}PhSO_3Na$), sodium alkyl benzene sulfonate with an average alkyl chain length of C12, and a commercial sulfonated glyceryl alcohol ethoxylate. The influence of the electrolyte concentration on the disjoining pressure is in perfect agreement with the observations made for SDS. With increasing salt concentration the stability of the CBF film increases until a CBF–NBF transition is observed at salt concentrations between 0.2 and 0.3 M, depending on the surfactant. Furthermore, $\Pi(h)$ curves at different surfactant concentrations were measured and interpreted in terms of the DLVO theory [79]. At surfactant concentrations below the cmc, excellent agreement between experiment and theory was found using the model of constant surface charge. The increase of the surfactant concentration results in an increase in both the film stability and its thickness, i.e. an increase in the surface charge density. However, above the cmc the theoretical $\Pi(h)$ curves were shifted by about 10 nm towards lower thicknesses at all pressures. The reason for this shift is not clear.

The cationic surfactants investigated so far are a series of alkyl trimethylammonium bromides ($C_n$TAB) as well as the dimeric surfactant ethanediyl-1,2-*bis* dodecylammonium bromide (12–2–12). For one of the $C_n$TAB surfactants, namely $C_{16}$TAB, Kolarov *et al* [50] found a charge reversal from negative to positive at the air/water interface at very low surfactant concentrations ($c < 10^{-7}$ M) due to the increased adsorption of $C_{16}$TAB. The 'nullifying' of the charge results in unstable films, before a further increase of the $C_{16}$TAB adsorption leads to an increase of the positive charge which eventually becomes high enough to stabilize the film. However, the instability at low surfactant concentrations is a consequence not only of the low charge but also of the low surface concentration. A pure water film is unstable mainly due to the absence of surfactant, i.e. to its low surface elasticity. The same holds for surfactant films at very low concentrations—a certain amount of surfactant is required to stabilize a film irrespective of the charge. In addition to the equilibrium thicknesses investigated by Kolarov *et al*, Bergeron [12] measured one complete $\Pi(h)$ curve of $C_{16}$TAB at the cmc (0.9 mM). Although Kolarov *et al* measured in the presence of 0.5 mM NaCl, the same maximum potential is observed, namely $125 \pm 15$ mV [50] and 145 mV [12], respectively. This agreement justifies the proposition that each surfactant has a characteristic maximum surface potential (table 3.2 in [23]). A classification of the surfactants according to the maximum surface potential obtainable would be very helpful for numerous applications. (Note that a characteristic surface potential does not imply a characteristic surface charge. Whereas the characteristic surface potential is constant over a wide range of electrolyte (salt and/or surfactant) concentration, the surface charge increases with increasing electrolyte concentration according to equation (4).) In the systematic work of Bergeron [12] it is not the $\Pi(h)$ curve of $C_{16}$TAB that is focused on but the influence of the surfactant chain length on the surface forces and the stability of thin liquid films. It was found that the chain length does not affect the forces but only the stability—a result which was also observed for a series of non-ionic surfactants some years later [58]. For highly purified $C_n$TABs an abrupt increase in film stability is seen when extending the chain length from $C_{12}$TAB to $C_{14}$TAB. In the presence of an uncharged cosurfactant this transition takes place between $C_{10}$TAB and $C_{12}$TAB. These transitions are discussed in terms of the surface elasticity which plays a stabilizing role by dampening both spatial and density fluctuations. The $C_n$TAB study reveals in a convincing way that similar forces do not result in similar film stabilities. It is the system's ability to resist disturbances that has to be taken into account. The appropriate parameters for quantifying this ability are still not defined.

A comparative study of the cationic dimeric surfactant ethanediyl-1,2-*bis* dodecylammonium bromide (12–2–12) and the corresponding monomeric $C_{12}$TAB leads to surprising

results [80]. First, very stable films are obtained with the 12–2–12 surfactant in contrast to the unstable $C_{12}$TAB films. A classical DLVO treatment cannot explain this difference. In the two cases, the attractive van der Waals forces are the same, whereas the repulsive force is much greater for $C_{12}$TAB than for 12–2–12 (95 versus 43 mV). Thus the DLVO theory predicts exactly the opposite of the experimental observations. It is again the surface elasticity that comes into play, underlining the need for appropriate parameters for quantifying this value (see discussion at the end of section 3.2). A second surprising observation is the fact that the addition of salt to a 12–2–12 solution (0.03 M at the cmc) leads to a CBF–NBF transition, which has not been observed for cationic systems so far. One explanation may be the very low surface charge density at the 12–2–12 interface (see below) which results in a low force barrier for the CBF–NBF transition. Last but not least, it has to be mentioned that all $\Pi(h)$ curves of the above-mentioned cationic surfactants can be very well described with the DLVO theory, which contrasts with the observations made for the anionic surfactants. However, the data available so far are not sufficient for judging whether or not this is purely by chance.

Although the surface charge density $q_0$ in the presence of ionic surfactants is one order of magnitude as higher compared to the non-ionic films, it is still very low with respect to the surface concentration. In other words, the surface charge density is much lower than the total amount of surfactant at the interface. The reason is the condensation of counterions, i.e. an incomplete dissociation of the surfactant. The effective surface charge can be calculated either from fitting the $\Pi(h)$ curve or simply from the measured equilibrium thickness. Subsequently, one can estimate the degree of dissociation from the DLVO parameters in combination with the adsorption isotherms. For example, it is known from surface tension measurements that the molecular area at the surface in a 3.5 mM $C_{14}$TAB solution is about 0.46 $nm^2$. The comparison of this value with the calculated surface charge of 46 mC $m^{-2}$ leads to the conclusion that only 13% of the surfactant molecules adsorbed at the surface are dissociated [12]. Even lower values were found for $C_{16}$TAB, where only 8% are dissociated. It is assumed that the origin of these low degrees of dissociation is the roughness of the interface. It was derived from neutron reflectivity data (see [21–28] in [12]) that a significant proportion of the surfactant head-groups are located in the hydrocarbon-rich region of the surfactant tails. Since the dielectric constant in the hydrophobic tail region is expected to be lower than that of the bulk aqueous solution, the dissociation in the interfacial region will be less favourable. This argument is underlined by the observation that the surface charge in a film stabilized by the dimeric surfactant 12–2–12 is as low as 4.7 mC $m^{-2}$ corresponding to a degree of dissociation of only 1% [80]. Due to the presence of the hydrophobic spacer at the interface, a lower hydration of the head-groups and thus a more hydrophobic interfacial region is assumed, which favours the condensation of counterions. It is only recently that a detailed review article was written about the adsorption of ionic surfactants at fluid interfaces [81]. It was shown that for the interpretation of experimental adsorption isotherms the introduction of counterion binding in the adsorption models is needed. From the best fit of experimental data to the theory developed by Kalinin and Radke [82] and by Kralchevsky *et al* [83], degrees of dissociation of 10–20% were found at the water/air interface. These data are in good agreement with the results obtained from the interpretation of the surface forces acting in thin liquid films.

As for the non-ionic surfactants, only a few studies deal with the influence of added surface-active components to get deeper insight into the properties of commercial surfactants. In this context, it was shown that highly purified $C_{12}$TAB does not stabilize thin liquid foam films, whereas with the unpurified surfactant as well as with small amounts of added dodecanol, stable $C_{12}$TAB films were obtained [12]. However, no difference was seen between purified and unpurified $C_{14}$TAB solutions. What is of crucial importance is that for the $C_n$TAB series small

amounts of impurities do not affect the surface forces, only the stability. A similar observation was made for the surfactant sodium 1-octanesulfonate ($C_8SO_3Na$). Whereas the pure $C_8SO_3Na$ produces very unstable foams, the addition of small amounts of octanol stabilizes the foam [72]. In contrast to the results obtained for the $C_n$TABs, the hydrolysis of SDS, which leads to the formation of dodecanol, has an influence on the thickness and thus on the forces of the SDS films. However, this influence has not been quantified yet. To sum up, one can say that systematic work on the influence of added surface-active components is needed. It is not only the influence of long-chain alcohols that is of interest, but also that of different surfactants. A lot of situations can be thought of which may be very important for the formulation of new products. For example, the surface charge and thus the thickness of films stabilized by non-ionic surfactants can be altered by the addition of ionic surfactants. In the case of ionic foam films, charges can be compensated by surfactants of opposite charge, which leads to a destabilization, whereas the addition of non-ionic surfactants could increase the stability. The challenge is to control the surface forces and the film stability independently by tuning the appropriate parameters.

## 4. Structural forces

Free-standing films are interesting in two respects. First, these single films can be considered the building blocks of a foam, so their properties affect the behaviour of the whole macroscopic foam, for example its stability. Second, the free-standing film presents a cavity which allows study of the effect of geometrical confinement on the structuring of colloidal particles, aggregates, or macromolecules. The liquid free-standing film is highly relevant in this respect, since its thickness can easily be varied by changing the outer pressure. The effect of the confinement on the ordering or structuring of molecules, particles, or aggregates is the objective of the following section.

### *4.1. What are structural forces?*

The confinement of a fluid between two walls induces a layering of molecules or particles. Such a layering is related to an oscillatory decay of the particle or molecule concentration from the interface towards the film bulk, which itself induces a damped oscillatory disjoining pressure. However, while the decaying oscillatory concentration profile near the film interfaces is well understood and has been calculated in detail (e.g. [84, 85]), the relation between this profile and an oscillatory disjoining pressure is still under discussion [86–88]. To illustrate the oscillatory disjoining pressure, in figure 7 an exponentially decaying cosine function is used for a simulation of the experimental data. The oscillatory or so-called 'structural' forces have been discussed in detail in [49]. Depending on the chosen molecules, these forces are also called solvation or hydration forces [89]. They cannot be described by the DLVO theory as they are due to the expulsion of molecules from the thin film. This expulsion induces an attractive depletion force since the concentration within the film is lower than in the corresponding reservoir for a short time. Due to the constant period of the forces, it is assumed that each time the same amount of material is squeezed out of the film. The period is somehow related to a characteristic length of the confined system like the diameter in the case of spherical molecules, particles, or aggregates (sections 4.2 and 4.3), or the correlation length between adjacent linear polyelectrolyte chains (section 4.4).

The liquid film between two solid interfaces can be investigated in an atomic force microscope (AFM) and in a surface force apparatus (SFA) while one between two liquid interfaces can be investigated in a TFPB (see section 2.1.1). With the exception of the surface

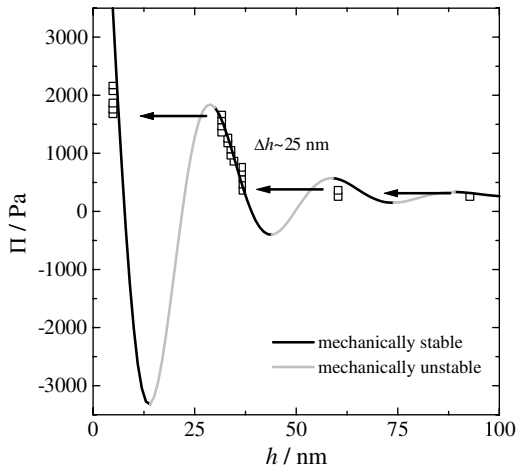


**Figure 7.** Disjoining pressure Πg as a function of the film thickness $h$ of a $C_{12}G_2$/PDADMAC film and its simulation by a damped oscillatory function. The mechanically stable and unstable parts are marked. In a TFPB experiment only the mechanically stable parts are accessible while in AFM and SFA experiments for suited systems the whole oscillation can be measured. The figure is adapted from [123].

roughness (see at the end of this section), the properties of the interfaces do not play a decisive role in the structuring of the confined fluid. Therefore, the results of AFM, SFM, and TFPB measurements can be compared. Introductions to these three methods are not given because they are outside the scope of the present review. Detailed descriptions can be found in other reviews (e.g. [6, 40]). However, for a thorough understanding of the present review, the most important differences between those three methods have to be mentioned.

(1) According to the Derjaguin approximation [49, 90] the disjoining pressure is proportional to the mathematical deviation of the force. This means that high disjoining pressures (TFPB) do not necessarily correspond to high forces (AFM, SFA), which makes it difficult to compare the results produced by the different methods. For instance, small forces could correspond to high pressures if the slope of the force curve is steep. In this particular case, the small forces are hard to detect, while the high pressures are easily measurable which could lead to the erroneous assumption that one method is more sensitive than another.
(2) The ranges of the oscillatory pressures are different. Whereas in the TFPB the pressure range for stratification is limited to $\Pi < 2000$ Pa, the corresponding pressure range accessible with the SFA is around 10 000 Pa. The difference originates most probably in the physical difference of the surfaces. Solid surfaces can support a large stress without deformation and hence minimize surface irregularities. In contrast, the spatial undulations of the fluid interfaces disrupt the supramolecular ordering responsible for the oscillatory structural force. The importance of surface roughness is described at the end of this section.
(3) With an AFM and a SFA the complete oscillation is measurable, while in the TFPB only the mechanically stable parts ($d\Pi/dh < 0$) are accessible. This is due to the fact that during the TFPB measurements the thickness is measured at a certain (given) capillary pressure. Therefore, in TFPB experiments only the repulsive parts (marked in black in figure 7) of the $\Pi(h)$ curve are measurable but not the attractive ones (mechanically unstable), which leads to steps in the film thickness. In contrast to this, in an AFM or SFA experiment each

value of the thickness can be adjusted, and the force (attractive or repulsive) is measured for each thickness, which leads to a continuous curve. However, a discontinuous curve can be also obtained with an AFM or a SFA if the force is the variable, and the thickness is measured like in the TFPB experiment. Of course, in theoretical calculations the variable can be freely chosen (thickness or force) [91], and both kinds of curve (continuous and discontinuous) can be simulated.

(4) Apart from the possibility of measuring attractive forces, another advantage of AFM and SFA is that almost all systems can be investigated while in the TFPB the film stability is the limiting factor for the choice of the compounds. An important advantage of the TFPB method is the fact that the surface charges can easily be changed and that there is no lavish surface preparation.

The oscillatory forces only occur if the molecules or aggregates are ordered both perpendicular and parallel to the surfaces over a reasonably long range (e.g. [92]). This means that the surface roughness and therefore the internal roughness between adjacent layers of molecules must be much lower than the period of the force oscillation. An expulsion only occurs if the distance $h_c$ between the two interfacial layers is commensurable with respect to the oscillation period $l$:

$$h_c = nl. \tag{6}$$

If the interfaces are rough, the distance between the interfaces varies in lateral direction $(x, y)$:

$$h_c = nl + \varepsilon l, \qquad 0 < \varepsilon(x, y) < 1, \tag{7}$$

and $h_c$ is not commensurable with respect to the period at certain lateral positions. If the precondition for layer expulsion is given only at a few positions in the film, no expulsion and thus no oscillatory force will be observed.

### *4.2. Spherical molecules, hard colloidal particles, and liquid crystals*

The ordering of molecules, particles, or aggregates leads to the so-called structural forces. Spherical molecules are entrapped e.g. between two mica plates in a SFA and the approach of the plates leads to damped oscillatory forces [93] which had been predicted for hard-sphere fluids before [94]. These results are explained by a layering of the molecules parallel to the mica surfaces which are squeezed out of the slit-pore layer by layer with increasing force. Oscillatory forces have also been observed for carbon chains which are assumed to be folded in the slit-pore. In this case, one oscillation corresponds to an unfolding process [95]. To sum up, one can say that the period of the oscillation is connected to a molecular length: the diameter of a spherical molecule or the diameter of a chain.

Oscillatory forces also occur in thin films of molten salt [96], liquid crystals [97], or colloidal particles [98–100]. The molecules or particles can be considered form-invariant hard spheres. For instance, AFM measurements on a solution of silica and/or sulfonated polystyrene particles entrapped between a silica microsphere and a flat silica plate show that with increasing diameter, increasing surface potential, and increasing concentration of the particles the force oscillation becomes more pronounced (i.e. the minima become deeper and the maxima higher) [101]. A curved film stabilized by silica particles also shows stratification due to the expulsion of the silica particles [88]. In this case the film is formed on a gas-filled capillary where the external pressure is changed in an asymmetric way.

Oscillatory forces of liquid crystals which are entrapped between two solid surfaces have been calculated by theoretical models [102]. The calculation of structural forces between planar surfaces immersed in a hard-sphere-like fluid shows that the pair correlation

function is a unique function of the particle bulk volume fraction and the particle hard-core diameter [103].

### *4.3. Micellar systems*

Structural forces also occur in aqueous films containing ionic surfactant at concentrations above the cmc, where micelles are formed. The micellar systems were investigated in a SFA between solid interfaces [104] and in a TFPB between liquid interfaces [5, 105–107], respectively. Similar observations have been made for a water-in-oil microemulsion of water–heptane–AOT, i.e. for an oil film containing inverse micelles [108]. It is assumed that the polydispersity of the micellar system reduces the amplitude of the force oscillation.

In contrast to those of spherical molecules and hard colloidal particles, the diameters of the micelles depend on thermodynamic conditions and are not form invariant. This peculiarity has to be considered if parameters such as the temperature, the pressure, and the composition are changed. In the case of the micellar system the step size scales with the surfactant concentration $c_s$ as $c_s^{-1/3}$ [109]. This can be simply explained by a homogeneous distribution of 'hard spheres' in three dimensions where the distance between two centres of mass is determined by the concentration of spheres. The step size is related to the diameter of the micelles plus twice the Debye length, the latter being affected by the degree of dissociation of the ionic surfactant and the ionic strength. In other words, the step size is related to an 'effective diameter'. From this diameter an effective volume fraction can be calculated. It has been found [104, 108] that effective volume fractions of at least 20 vol% are required to observe structural forces, irrespective of the surfactant used. Under this assumption, the main difference between non-ionic and ionic surfactants could be the amount of surfactant needed to observe structural forces. In the case of non-ionic surfactants, the micellar volume fraction has to be equal to the 'critical' volume fraction, whereas in the case of ionic surfactants the micellar volume fraction, which is required to see structural forces, depends on the Debye length. Thus, keeping the surfactant concentration constant, one observes with increasing salt concentration that the steps become smaller and vanish at a certain ionic strength. In the image of the effective volume which could be decisive for oscillatory forces, the effect of increasing ionic strength is due to the effective diameter of the micelles and thus the effective volume of the dispersed phase decreasing until it is too low to induce structural forces.

Beside surfactants of low molecular mass, also amphiphilic triblock copolymers [110, 111] of the type ABA (A: hydrophilic; B: hydrophobic) or amphiphilic diblock copolymers [21, 112–115] of the type AB stabilize free-standing films. The hydrophobic part is collapsed at the air/water interface, and the hydrophilic part forms a brush directed towards the solution (see figure 8(a), left side). The brush-like structure at the film surfaces is derived from ellipsometry and x-ray reflectometry measurements for a single air/water interface [43, 116]. With increasing ionic strength the film becomes thinner owing to the screening of the electrostatic repulsion between the equally charged film surfaces. (This is also observed for films of small surfactant molecules; see section 3.) Furthermore, charged hydrophilic blocks coil with increasing ionic strength, which also provides a contribution to film thinning (see figure 8(a), right side). This class of block copolymers behave like large surfactant molecules. Above a certain polymer concentration a stepwise thinning occurs again, and the step size corresponds to the diameter of a micelle in the corresponding solution [114, 117]. These findings suggest the interpretation that a layer of diblock copolymer micelles is entrapped within the film and is squeezed out (figure 8(b)). The structuring of the polymer micelles within the film seems to be weaker than the structuring of micelles consisting of low-molecular-mass surfactant, since the pressure which is needed to induce a step in film thickness is much lower.

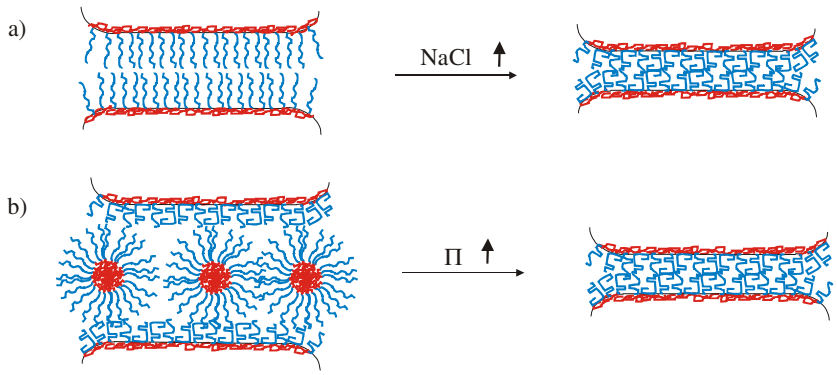


**Figure 8.** Assumed structures of a foam film stabilized by amphiphilic diblock copolymers. (a) The approach of two brushes at low polymer concentration and the influence of ionic strength. (b) Expulsion of one layer of micelles at a high polymer concentration. The figure is adapted from [114].

### *4.4. Polyelectrolyte/surfactant films*

Free-standing films made from aqueous surfactant/polyelectrolyte solutions and investigated in a TFPB also show structural forces above a certain polyelectrolyte concentration (e.g. [30, 118–123]). In films containing oppositely charged polyelectrolytes and surfactants, surface complexes between the two classes of compounds are formed at surfactant concentrations above the critical surface aggregation concentration (csac). This has been detected by a reduction in surface tension [124, 125], and by x-ray and neutron reflectometry [126, 127]. Usually, in this class of mixed films the surfactant concentration is below the critical aggregation concentration (cac) in the bulk, which is itself below the cmc of the pure surfactant. Above the cac the film is not homogeneous any longer and shows a crystalline-like structure [128]. The formation of surface-active polyelectrolyte/surfactant complexes increases the film stability, since the pure surfactant films are not stable at these low concentrations [118, 128]. However, polyelectrolytes stabilize the foam films even in the absence of surface-active complexes, which is the case if both compounds are identically charged or if the surfactant is neutral. In this case, the stabilizing effect is due to oscillatory forces which might hamper the film drainage [129].

Different combinations of surfactants and polyelectrolytes have shown that the choice of the surfactant has an influence on the total film thickness [130], but no influence on the step size of the disjoining pressure isotherms [119, 122, 123]. In [119, 130] it is shown that the step size remains constant for a certain polyelectrolyte at a fixed concentration irrespective of whether the polyelectrolyte is adsorbed at the interface or not. In the following it will be shown how the molecular architecture (section 4.4.1) and the electrostatic interactions (section 4.4.2) between these chains influence the stratification behaviour.

#### *4.4.1. Influence of molecular architecture.*

*Branched polyelectrolytes:* Foam films formed from aqueous solutions containing the non-ionic surfactant dodecyl-$\alpha$-D-maltoside ($C_{12}G_2$) and the cationic polyelectrolyte poly(ethylene imine) (PEI) show a stepwise thinning [131, 132]. The PEI is irregularly branched and it is assumed to have an elliptic shape. The diameter is estimated from dynamic light scattering measurements [133]. Figure 9 shows the step size as a function of the corresponding concentration of monomer units for two different molecular weights. The step size $\Delta h$ scales

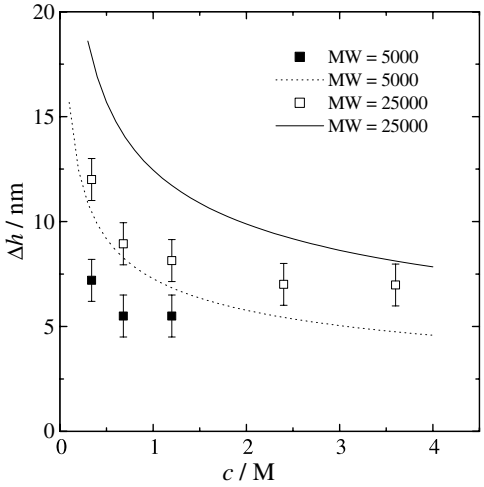


**Figure 9.** Step size $\Delta h$ of the film thinning and calculated distance (curves) between the PEI molecules in solution as a function of the polyelectrolyte concentration for two different molecular weights. The concentration is given in terms of the corresponding monomer concentration $c$. The experimental data are adapted from [131].

with the polyelectrolyte concentration as $c_p^{-1/3}$ [131]. In analogy with the spherical particles discussed above, a layer-by-layer expulsion is assumed. Furthermore, the step size increases with increasing molecular weight. The step size in the films can be estimated from two different simple models which are based on: (1) purely geometric arguments and (2) pure electrostatic repulsion between the molecules. First, the geometry is considered. At a *fixed* concentration $c$ of monomer units the step size increases with increasing molecular weight, since the effective concentration of polymer $c_p$ decreases and, therefore, the distance between the polymers increases. Simple geometric considerations enable us to calculate the average distance $d$ between two polymers in solution:

$$d = c_p^{-1/3} 2(3/(4\pi))^{1/3} \sim (2/c_p)^{1/3}. \tag{8}$$

This distance is indicated with curves in figure 9. The measured step sizes are smaller, which could be an indication that the PEI molecules are pressed together within the film. In addition to these geometric aspects, electrostatic repulsion between the PEI molecules seems to be important for their layering within the film (see section 4.4.2). Pure electrostatic repulsion between the branched polyelectrolytes would lead to a distance, and therefore to a step size, which corresponds to the diameter (about 3 nm for MW 5000 and about 5 nm for MW 25 000) plus twice the Debye length in analogy with the layering of charged micelles. However, the experimentally determined step size is much larger, and indicates a Debye length three to four times larger than the one calculated from the counterion concentration. This would mean a concentration of free counterions at least ten times lower. One reason could be that most of the counterions are not free, but entrapped within the branched polyelectrolyte. Furthermore, the degree of dissociation of the weak PEI could be reduced in the confined geometry of the film, which also reduces the ionic strength. If the origin for stratification were pure electrostatic repulsion between the PEI molecules, only the Debye length would be influenced by the polyelectrolyte concentration, which itself scales with the concentration of free counterions as $\sim c_{el}^{-1/2}$. This is not consistent with the exponent of $-1/3$ obtained for the scaling behaviour of the steps from the experimental curves. An explanation for this mismatch might be the

ratio between free and entrapped counterions which could change with the polyelectrolyte concentration. Work on this question is under way.

*Linear polyelectrolytes:* Foam films containing linear polyelectrolytes also show a stepwise thinning. This has been observed for both negatively charged polyelectrolytes [118, 119, 121, 122, 128] and polycations [30, 120, 123]. In contrast to the case for branched polyelectrolytes the step size scales with the polyelectrolyte concentration as $\Delta h \sim c_p^{-1/2}$. This stratification behaviour is independent of the persistence length and is observed not only for flexible and semi-flexible chains [121] but also for worm-like micelles [80] which can be regarded as 'living' polymers. A $\Pi(h)$ curve of the positively charged poly(diallyl-dimethyl ammonium chloride) (PDADMAC) and $C_{12}G_2$ is shown in figure 7. At a certain polyelectrolyte concentration the film starts to thin stepwise. The steps are irreversible. On decreasing the pressure no step backward to the former branch of the $\Pi(h)$ curve is possible, and the thickness does not change in a significant way. Since the surfactant is non-ionic it is assumed that there is no strong aggregation between the surfactant and the polyelectrolyte. The measurements were also carried out at other polyelectrolyte concentrations, and the general result is that the number of steps increases with increasing polyelectrolyte concentration and the steps become smaller.

The experimental data can be interpreted as parts of a damped oscillation, as shown in figure 7. With increasing polyelectrolyte concentration the minima and maxima of the oscillations become more pronounced (e.g. [118, 119]). The step size and the film thickness at which a certain step occurs become smaller. At extremely high polyelectrolyte concentrations the effect of the counterions becomes important [122], which reduces the amplitude of the oscillation (see the section on the effect of the ionic strength).

The *attenuation* explains the *irreversibility* of the steps. If the system is at a mechanically unstable point after an increase of the pressure, it jumps into the next mechanically stable state, which is the next thinner isotherm branch. On the other hand, if the pressure is decreased, the system remains mechanically stable and has no 'motivation' to jump back to the former thicker isotherm branch. In connection with the stratifications of films containing hard colloidal particles where the steps in film thickness are somehow related to the diameter of the particles, the question arises of which characteristic length corresponds to the period of the oscillatory curve. By analogy with the systems discussed above, one could assume that the period is related to the radius of gyration. This would mean that the step size should change with the degree of polymerization. But the TFPB measurements show no effect of the chain length on the step size, which means that a layering of polyelectrolyte coils cannot be the right model. To check the influence of other characteristic polymer lengths the corresponding aqueous polyelectrolyte *solutions* have been investigated by means of small-angle scattering (SANS or SAXS). The scattering spectra show a broad peak, which indicates an interaction between the chains [113, 122, 123, 134–138]. The peak position $q_{max}$ shifts to higher $q$-values with increasing polyelectrolyte concentration. In contrast to the case for experiments with branched polyelectrolytes it is the corresponding monomer concentration $c$ and *not* the polyelectrolyte concentration $c_p$ that has to be considered. This is explained below in connection with the isotropic model of overlapping chains. Under the assumption that the Bragg equation can be applied, $q_{max}$ can be transformed into a length $\xi$ via

$$\xi = 2\pi/q_{max} \tag{9a}$$

$$q_{max} \propto c^{1/2}. \tag{9b}$$

Note that equation (9*b*) results from the correlation between $\xi$ and the concentration $c$, which differs for strongly (equation (10)) and weakly (equation (11)) charged polyelectrolytes. The

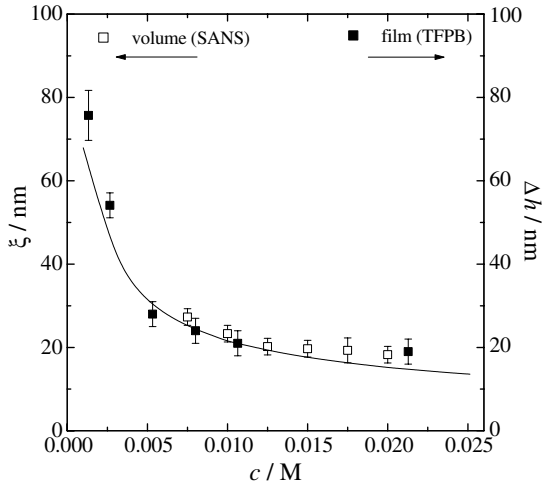


**Figure 10.** Comparison between the step size $\Delta h$ of the film thinning of a free-standing $C_{12}G_2$/PDADMAC film measured in a TFPB and the correlation length $\xi$ of the respective aqueous PDADMAC solution measured by means of SANS (calculated from the position of the structure peak in SANS spectra using equation (9*a*)). $\Delta h$ and $\xi$ are plotted as a function of the polyelectrolyte concentration. The concentration is given in terms of the corresponding monomer concentration $c$. The solid curve is a simulation of the correlation length according to equation (10) ($b = 3.6$ Å). The experimental data are adapted from [123].

scaling behaviour of the peak position with the polyelectrolyte concentration has been predicted by the isotropic model [139–143] which assumes an overlapping of the chains above a certain polymer concentration $c^*$ (semi-dilute regime). A kind of transient network is formed, where the correlation length $\xi$ corresponds to the mesh size and the peak width in the scattering spectrum to the polydispersity of the mesh sizes. With increasing polyelectrolyte concentration, also the concentration of counterions increases. This leads to an enhanced electrostatic screening between the chains, which is related to a broadening of the correlation peak [123]. A comparison between the correlation length obtained from small-angle scattering measurements with the step size in the disjoining pressure isotherms shows that the two lengths are similar (figure 10). This was shown for the first time in [113] and it has been described in other publications since [122, 123]. This means that the interactions between the polyelectrolyte chains which induce a structuring of the chains in the aqueous solution are the same as the interactions in the film which lead to the film stratification. Under the assumption that the polyelectrolyte chains form a network-like structure in aqueous solution, this structure can obviously be transferred to the film bulk. Other authors assume that the polyelectrolytes are close-packed cylindrical objects within the film [122]. In analogy with charged micelles, the step size would correspond to the diameter of the molecules plus twice the Debye length, then. This contrasts with the fact that the calculated diameter of the 'effective' cylinders is much smaller than the measured step size [119].

Hence, the period of the oscillatory disjoining pressure curve corresponds to the correlation length found in the bulk solution. The isotropic model of overlapping chains, which has been explained above, predicts the correlation length $\xi$ for solutions of strongly charged polyelectrolytes ($l_B/b > 1$) and for weakly charged polyelectrolytes ($l_B/b \ll 1$). Both classes of polyelectrolytes are distinguished by the distance $b$ between two adjacent charges in comparison with the Bjerrum length $l_B$ which presents the distance between two ions in a solvent where the Coulomb energy equals the thermal energy. In water, this distance is 7.1 Å.

If the charge distance is shorter than the Bjerrum length, counterion condensation takes place [144–146] until the 'effective' charge distance equals the Bjerrum length. According to [140, 141] the correlation length of strongly charged polyelectrolyte solutions is

$$\xi \sim bc^{-1/2}, \tag{10}$$

where $b$ is the distance between two adjacent charges along the chains. In the case of a weakly charged chain where one monomer carries one charge among $\sigma$ uncharged monomers, the correlation length is given by [147]

$$\xi \sim \left(\frac{\sigma^{4/7}}{(l_B/a)^{2/7}ac}\right)^{1/2}, \tag{11}$$

where $a$ is the monomer size. The correlation lengths calculated using these equations for the respective polyelectrolytes are in good agreement with the step size in the $\Pi(h)$ curves and therefore also with the bulk correlation length determined from SANS measurements [119, 121]. One example for a strongly charged polyelectrolyte is given in figure 10. In contrast to the case for branched polyelectrolytes, the step size does not depend on the molecular weight. This is a further indication of a network-like structure within the film, since it is on the monomer concentration and not on the chain length that the mesh size in the isotropic model depends.

In comparison with layered sphere-like particles or molecules described in the earlier sections, the expulsion of polyelectrolyte chains is more difficult to imagine. From fluorescence measurements on foam films containing dye-labelled polyelectrolytes, it is known that the polyelectrolyte chains are pressed out of the film and that they are not collapsed within the film [30]. This means that as many monomers as belong to one mesh size are expelled during a certain transition from a thicker to a thinner film. However, as one polyelectrolyte chain may be involved in several meshes it is not simply one chain that is expelled. The idea is that the network breaks down and is rebuilt much faster than the time resolution of the TFPB [123]. Up to a certain pressure the network rebuilds itself with $n$ meshes in the film, and above this pressure the network is only rebuilt with $n - 1$ meshes. Thus, before the transition the total film thickness equals $h_t$, which is reduced to $h_t - \xi$ after the stepwise thinning process. The following equations hold:

$$h_t = 2h_s + h_c = 2h_s + n\xi, \tag{12a}$$

$$h_t - \xi = 2h_s + (n-1)\xi, \tag{12b}$$

where $h_c$ is the thickness of the film core, and $h_s$ is the thickness of one surface layer. The polyelectrolyte chains which are not involved in the network any longer are pressed out of the film. Therefore the polyelectrolyte concentration is reduced in comparison with the concentration in the surrounding meniscus, which induces (attractive) depletion forces between the film surfaces with the result that the film thins out stepwise. Using this model would mean that the mesh size is the same in solution and in the film and that the film does not represent a confined geometry with respect to the mesh size. This could be explained by image charges which extend the network to infinity [131]. Furthermore, at low concentrations the surfactant has no effect on the step size, which means that the interactions between polyelectrolytes and surfactant are negligible. This has also been observed by means of SANS measurements on aqueous polyelectrolyte solutions, where the position of the structure peak is not influenced by the addition of surfactant [122, 123].

Milling *et al* [148–150] observed oscillatory forces within aqueous solutions of linear polyelectrolytes with an AFM. They were the first to find that the correlation length of these forces scales with $c^{-1/2}$. With SFA measurements, however, no force oscillation for polymers

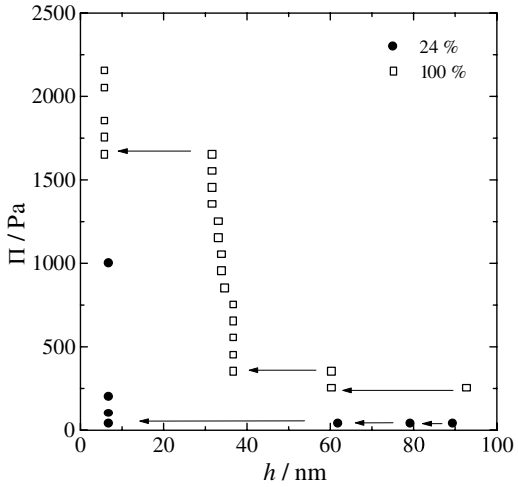


**Figure 11.** Disjoining pressure Π as a function of the film thickness $h$ for APG/PDADMAC films at two different degrees of PDADMAC charge: 100% (fully charged chain) and 24%. The data are adapted from [120].

has been published, which might be due to the differences between the TFPB and SFA, which were discussed in section 4.1. Oscillations in the concentration profile of a polymer system between two interfaces are predicted by theoretical models [151, 152], but to our knowledge there have not yet been any simulations of oscillatory forces of polyelectrolyte solutions entrapped between two interfaces.

*4.4.2. Influence of electrostatics.* Both decreasing the charge density along the polyelectrolyte chain and increasing the concentration of low-molecular-weight salt lead to a reduction of the pressure which is necessary to induce a step in the film thickness. At a high ionic strength or at a low degree of charge the stratification vanishes [118, 120]. In the following the effect of the polymer charge density and the ionic strength will be discussed.

*Effect of polymer charge density:* Figure 11 shows the isotherms of a film containing the strong polyelectrolyte PDADMAC at different degrees of charge. The charge density is changed by varying the ratio between cationic diallyl-dimethyl ammonium chloride (DADMAC) monomers and neutral *N*-methyl-*N*-vinylacetamide (NMVA) units. Above a degree of charge of about 50% the disjoining pressure isotherms look quite similar [120]. The steps occur one after the other at different pressures and the step sizes are quite similar. Below a degree of charge of 50% all steps occur at the same low pressure. This leads to the conclusion that the electrostatic repulsion between the polyelectrolyte chains is reduced and that the structuring becomes 'softer' at a low polymer charge density. SANS measurements on the corresponding polyelectrolyte solutions result in a correlation length which increases with decreasing degree of charge [123]. This is assumed to be caused by stronger coiling of the chains owing to less repulsion between the charges along the chain. If one projects the coiled chain on a line, both the 'effective' length and the 'effective' number of monomer units per chain decrease. Therefore, the effective monomer concentration also decreases, which in turn increases the correlation length [139, 147, 153, 154] in agreement with equations (10) and (11). An indication of an increase in step size with decreasing degree of charge is also observed in

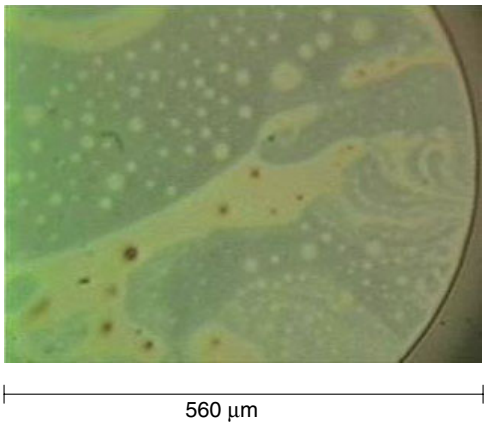


**Figure 12.** A foam film of $C_{12}$TAB and 45% charged PSS (P($S_{0.55}$-*stat*-$SS_{0.45}$)). The inhomogeneities are caused by aggregates between different polyelectrolyte chains due to hydrophobic parts in the polymer backbone [155].

the disjoining pressure isotherms. Since at low pressures the different thicknesses between the steps cannot be stabilized in the TFPB measurements, only qualitative statements are possible. The advantage of the statistical copolymer P(DADMAC-*stat*-NMVA) is that it is water soluble over the whole range of polymer charge density (0–100%) and that it produces foam films of a homogeneous thickness. In contrast to this polyelectrolyte, poly(styrene sulfonate sodium salt) (PSS) at a degree of charge below 60% induces gel-like aggregates in the films [122, 155] (figure 12), which is due to hydrophobic parts along the polymer chain making it difficult to get reproducible $\Pi(h)$ curves. However, the advantage of a statistical poly(styrene-*stat*-styrene sulfonate sodium salt) is that the (poly(styrene)) backbone does not change with variation of the charge density as is the case for P(DADMAC-*stat*-NMVA).

In the case of weak polyelectrolytes, such as PEI, the charge density has been changed by pH variation, and the pressure which is needed to induce a step decreases again with decreasing polymer charge density [131]. The comparison between the disjoining pressure curves of branched and linear PEI shows that in the case of the linear one the steps are induced at a lower pressure than in the case of the branched one, which could be due to a higher charge density of the branched PEI in comparison to the linear one: the number of charged monomers at a certain pH is almost independent of the degree of branching [131], but the volume of a branched PEI molecule is much smaller than that of a swollen coil of linear PEI.

The fact that the $\Pi(h)$ curve is independent of the degree of charge above 50% is due to the so-called charge renormalization. In the case of fully charged PDADMAC the charge distance is about the half of the Bjerrum length which means that the counterion condensation takes place at a degree of charge between 50 and 100%. Therefore, in this regime both the effective charge distance and the concentration of free counterions are constant. This explains why the film thickness between two steps in the isotherms is independent of the polymer charge density between 50 and 100%. The thickness is extremely sensitive to the ionic strength, as has been mentioned in section 3. This effect of charge renormalization has also been observed by means of small-angle scattering measurements in solution [123, 137]. The position of the structure peak is independent of the degree of charge above the counterion condensation threshold.

*Effect of ionic strength:* With increasing ionic strength the stratification of the film occurs at lower pressures [120]. It is noteworthy that this effect is already observed at salt concentrations below the concentration of polyelectrolyte counterions. Usually, in solution, salt effects become important only at salt concentrations above the concentration of polyelectrolyte counterions. This high sensitivity to the ionic strength seems to be induced by the geometrical confinement, but this effect has not been clarified yet. SANS measurements on the corresponding polyelectrolyte solutions show a more or less fixed peak position up to a salt concentration equal to the polyelectrolyte concentration [123, 137]. At higher salt concentrations the structure peak cannot be resolved due to a strong forward scattering (i.e. at low $q$-values) related to an increasing osmotic compressibility and a decreasing osmotic pressure.

## 5. Conclusions

Oscillatory forces occur in thin films containing e.g. particles, micelles, or macromolecules due to the oscillating concentration profile from the film interface towards the film core. This leads to a stepwise thinning of free-standing films investigated with a TFPB. The period of the oscillation is related to the diameter of the particles or aggregates and to the correlation length of the polymer system. The amplitude of the force oscillation increases with increasing concentration, and decreases with decreasing electrostatic repulsion between the structuring units. Some experiments indicate that a minimum 'effective' volume of the molecules, particles, or aggregates is the decisive factor for the occurrence of force oscillations. This would mean that at high enough concentrations, aggregates, particles, and macromolecules of all kinds should result in force oscillations, irrespective of their charge density or the ionic strength.

Another important aspect of structural forces is that the molecular architecture has a pronounced effect on the structuring of polyelectrolytes within free-standing films. The consequence is a different stratification behaviour of the free-standing films containing either linear or branched polyelectrolytes. Highly branched polyelectrolytes are assumed to be elliptical (or spherical) molecules. In analogy with particles or micelles, they are assumed to form layers which are squeezed out of the film with increasing pressure. The size of the steps $\Delta h$ in $\Pi(h)$ curves depends on the degree of polymerization and scales with the polyelectrolyte concentration as $c_p^{-1/3}$. The same scaling behaviour is observed for films containing spherical micelles. On the other hand, foam films containing linear polyelectrolytes show steps in film thickness whose size does not depend on the molecular weight and which scales with the polyelectrolyte concentration (or rather the corresponding monomer concentration $c$) as $c^{-1/2}$. The steps show the same size and the same scaling behaviour as the correlation length $\xi$ found for semi-dilute polyelectrolyte solutions, where a transient network-like structure of the polyelectrolyte chains is assumed. However, the correlation length detected in semi-dilute polyelectrolyte solutions is a statistical length, and the question that remains to be answered is how a statistical length can be detected by force or disjoining pressure measurements.

## Acknowledgments

Lively and fruitful discussions with Professors R Strey and P Claesson are gratefully acknowledged. C Stubenrauch is indebted to the *Fonds der Chemischen Industrie* and the *Ministerium für Wissenschaft und Forschung des Landes NRW* for financial support.

## References


[1] Bergeron V 1999 *J. Phys.: Condens. Matter* **11** R215
[2] Israelachvili J N and Wennerström H 1992 *J. Phys. Chem.* **96** 520
[3] Mysels K J and Jones M N 1966 *Discuss. Faraday Soc.* **42** 42
[4] Exerowa D and Scheludko A 1971 *C. R. Acad. Bulg. Sci.* **24** 47
[5] Bergeron V and Radke C 1992 *Langmuir* **8** 3020
[6] Claesson P M, Ederth T, Bergeron V and Rutland M W 1996 *Adv. Colloid Interface Sci.* **67** 119
[7] Scheludko A and Platikanov D 1961 *Kolloidn. Zh.* **175** 150
Scheludko A 1967 *Adv. Colloid Interface Sci.* **1** 391
[8] Duyvis E M 1962 *Thesis* Utrecht University
[9] Persson C M, Claesson P M and Johansson I 2000 *Langmuir* **16** 10227
[10] Persson C M, Claesson P M and Lunkenheimer K 2002 *J. Colloid Interface Sci.* **251** 182
[11] Stubenrauch C, Schlarmann J and Strey R 2002 *Phys. Chem. Chem. Phys.* **4** 4504
[12] Bergeron V 1997 *Langmuir* **13** 3474
[13] Bergeron V, Waltermo A and Claesson P M 1996 *Langmuir* **12** 1336
[14] Karraker K A and Radke C J 2002 *Adv. Colloid Interface Sci.* **96** 231
[15] Sentenac D, Schalchli A, Nedyalkov M and Benattar J J 1996 *Faraday Discuss.* **104** 345
[16] Sentenac D and Dean D S 1997 *J. Colloid Interface Sci.* **196** 35
[17] Sentenac D and Benattar J J 1998 *Phys. Rev. Lett.* **81** 160
[18] Stubenrauch C 2000 unpublished results
[19] Waltermo A, Claesson P M, Simonsson S, Manev E, Johansson I and Bergeron V 1996 *Langmuir* **12** 5271
[20] Toca-Herrera J L, Krustev R, Müller H-J and Möhwald H 2000 *Colloid Polym. Sci.* **278** 771
[21] Saint-Jalmes A, Sonin A A, Delsanti M, Guenoun P, Yang J, Mays J W and Langevin D 2002 *Langmuir* **18** 2103
[22] Tian G, Khrenov V, Tauer K and von Klitzing R 2000 unpublished results
[23] Exerowa D and Kruglyakov P M 1998 *Foam and Foam films—Theory, Experiment, Application* ed D Möbius and R Miller (Amsterdam: Elsevier)
[24a] Khristov K, Taylor S D, Czarnecki J and Masliyah J 2000 *Colloids Surf.* A **174** 183
[24b] Taylor S D, Czarnecki J and Masliyah J 2002 *J. Colloid Interface Sci.* **252** 149
[25] Exerowa D, Cohen R and Nikolova A 1987 *Colloids Surf.* **24** 43
[26] Exerowa D and Nikolova A 1992 *Langmuir* **8** 3102
[27] Nikolova A, Exerowa D, Lalchev Z and Tsonev L 1994 *Eur. Biophys. J.* **23** 145
[28] Cascao Pereira L G, Johansson C, Blanch H W and Radke C J 2001 *Colloids Surf.* A **186** 103
[29] Scheludko A and Exerowa D 1959 *Comm. Dept. Chem. Bulg. Acad. Sci.* **7** 123
Scheludko A and Exerowa D 1959 *Kolloidn. Zh.* **165** 148
Scheludko A and Exerowa D 1960 *Kolloidn. Zh.* **168** 24
[30] Toca-Herrera J L and von Klitzing R 2002 *Macromolecules* **35** 2861
[31] Aveyard R, Binks B P, Cho W-G, Fisher L R, Fletcher P D I and Klinkhammer F 1996 *Langmuir* **12** 6561
[32] Binks B P, Cho W-G and Fletcher P D I 1997 *Langmuir* **13** 7180
[33] Aveyard R, Binks B P, Esquena J, Fletcher P D I, Buscall R and Davies S 1999 *Langmuir* **15** 970
[34] Aveyard R, Binks B P, Esquena J, Fletcher P D I, Bault P and Villa P 2002 *Langmuir* **18** 3487
[35] Leal-Calderon F, Stora T, Mondain-Monval O, Poulin P and Bibette J 1994 *Phys. Rev. Lett.* **74** 2959
[36] Mondain-Monval O, Leal-Calderon F and Bibette J 1996 *J. Physique* II **6** 1313
[37] Espert A, Omarjee P, Bibette J, Leal-Calderon F and Mondain-Monval O 1998 *Macromolecules* **31** 7023
[38] Dimitrova T D and Leal-Calderon F 1999 *Langmuir* **15** 8813
[39] Dimitrova T D, Leal-Calderon F, Gurkov T D and Campbell B 2001 *Langmuir* **17** 8069
[40] Claesson P M and Kjellin U R M 1999 *Modern Characterization Methods of Surfactant Systems* ed B P Binks (New York: Dekker) p 255
[41] Saint-Jalmes A, Zemb T and Langevin D 2001 *Prog. Colloid Polym. Sci.* **118** 1
[42] Anklam M R, Saville D A and Prud'homme R K 1999 *Langmuir* **15** 7299
[43] Schillén K, Claesson P M, Malmsten M, Linse P and Booth C 1997 *J. Phys. Chem.* **101** 4238
[44] Hadjiiski A, Dimova R, Denkov N D, Ivanov I B and Borwankar R P 1996 *Langmuir* **12** 6665
[45] Hadjiiski A, Tcholakova S, Denkov N D, Durbut P, Broze G and Mehreteab A 2001 *Langmuir* **17** 7011
[46] Hadjiiski A, Tcholakova S, Ivanov I B, Gurkov T D and Leonard E 2002 *Langmuir* **18** 127
[47] Bergeron V, Fagan M E and Radke C J 1993 *Langmuir* **9** 1704
[48] Bergeron V and Radke C J 1995 *Colloid Polym. Sci.* **273** 165
[49] Israelachvili J 1998 *Intermolecular and Surface Forces* 2nd edn, 7th printing (San Diego, CA: Academic)

[50] Kolarov T, Yankov R, Esipova N E, Exerowa D and Zorin Z M 1993 *Colloid Polym. Sci.* **271** 519
[51] Usui S and Sasaki H 1978 *J. Colloid Interface Sci.* **65** 36
[52] Yoon R H and Yordan J L 1986 *J. Colloid Interface Sci.* **113** 430
[53] Balzer D 1993 *Langmuir* **9** 3375
[54] Marinova K G, Alargova R G, Denkov N D, Velev O D, Petsev D N, Ivanov I B and Borwankar R P 1996 *Langmuir* **12** 2045
[55] Li C and Somasundaran P 1991 *J. Colloid Interface Sci.* **146** 215
[56] Graciaa A, Morel G, Saulnier P, Lachaise J and Schechter R S 1995 *J. Colloid Interface Sci.* **172** 131
[57] Exerowa D 1969 *Kolloidn. Zh.* **232** 703
[58] Karraker K A 1999 *Thesis* University of California, Berkeley, CA
[59] Jungwirth P and Tobias D J 2002 *J. Phys. Chem.* B **106** 6361
[60] Manev E D and Pugh R J 1991 *Langmuir* **7** 2253
[61] Khristov K, Exerowa D and Yankov R 1997 *Colloids Surf.* A **129/130** 257
[62] Becher P and Schick M J 1987 *Nonionic Surfactants* ed M J Schick (New York: Dekker) p 435
[63] Kolarov T, Cohen R and Exerowa D 1989 *Colloids Surf.* **42** 49
[64] Pratt L R and Pohorille A 2002 *Chem. Rev.* **102** 2671
[65] Schlarmann J, Stubenrauch C and Strey R 2003 *Phys. Chem. Chem. Phys.* **5** 184
[66] Miller R, Wüstneck R, Krägel J and Kretzschmar G 1996 *Colloids Surf.* A **111** 75
[67] Langevin D 1998 *Curr. Opin. Colloid Interface Sci.* **3** 600
[68] Monroy F, Giermanska Kahn J and Langevin D 1998 *Colloids Surf.* A **143** 251
[69] Wantke K-D, Fruhner H, Fang J and Lunkenheimer K 1998 *J. Colloid Interface Sci.* **208** 34
[70] Fruhner H, Wantke K-D and Lunkenheimer K 1999 *Colloids Surf.* A **162** 193
[71] Langevin D 2000 *Adv. Colloid Interface Sci.* **88** 209
[72] Monin D, Espert A and Colin A 2000 *Langmuir* **16** 3873
[73] Exerowa D, Zacharieva M, Cohen R and Platikanov D 1979 *Colloid Polym. Sci.* **257** 1089
[74] Exerowa D, Kolarov T and Khristov Khr 1987 *Colloids Surf.* **22** 171
[75] Israelachvili J N and Adams G E 1978 *J. Chem. Soc. Faraday Trans.* 1 **74** 975
[76] Pashley R M and Israelachvili J N 1981 *Colloids Surf.* **2** 169
[77] Krustev R and Müller H-J 1999 *Langmuir* **15** 2134
[78] Müller H-J 2001 personal communication
[79] Black I J and Herrington T M 1995 *J. Chem. Soc. Faraday Trans.* **91** 4251
[80] Espert A, von Klitzing R, Poulin P, Colin A, Zana R and Langevin D 1998 *Langmuir* **14** 4251
[81] Fainerman V B and Lucassen-Reynders E H 2002 *Adv. Colloid Interface Sci.* **96** 295
[82] Kalinin V V and Radke C J 1996 *Colloids Surf.* A **114** 337
[83] Kralchevsky P A, Danov K D, Broze G and Mehreteab A 1999 *Langmuir* **15** 2351
[84] Schmidt M and Löwen H 1997 *Phys. Rev.* E **55** 7228
[85] Gao J, Luedtke W and Landman U 1997 *J. Phys. Chem.* B **101** 4013
[86] Kralchevsky P A, Nikolov A D, Wasan D T and Ivanov I B 1990 *Langmuir* **6** 1180
[87] Bergeron V, Jimenez-Laguna A and Radke C J 1992 *Langmuir* **8** 3027
[88] Sethumadhavan G N, Nikolov A D and Wasan D T 2001 *Langmuir* **17** 2059
[89] Israelachvili J and McGuiggan P M 1988 *Science* **241** 795
[90] Derjaguin B V 1934 *Kolloidn. Z.* **69** 155
[91] Schoen M 2001 personal communication
[92] Gee M L and Israelachvili J 1990 *J. Chem. Soc. Faraday Trans.* **86** 4049
[93] Horn R G and Israelachvili J N J 1981 *Chem. Phys.* **75** 1400
[94] Mitchell D J, Ninham B W and Pailthorpe B A 1978 *J. Chem. Soc. Faraday Trans.* II **74** 1116
[95] Christenson H K, Gruen D W R, Horn R G and Israelachvili J N 1987 *J. Chem. Phys.* **87** 1834
[96] Horn R G, Evans D F and Ninham B W 1988 *J. Phys. Chem.* **92** 3531
[97] Ivanov I B and Dimitrov D S 1988 *Thin Liquid Films* ed I B Ivanov (New York: Dekker) p 379
[98] Perez E, Proust J E and Ter-Minassian-Saraga L 1988 *Thin Liquid Films* ed I B Ivanov (New York: Dekker) p 891
[99] Basheva E S, Nikolov A D, Kralchevsky P A, Ivanov I B and Wasan D T 1991 *Surfactants in Solution* vol 11, ed K L Mittal and D O Shah (New York: Plenum) p 467
[100] Nikolov A D and Wasan D T 1992 *Langmuir* **8** 2985
[101] Piech M and Walz J Y 2002 *J. Colloid Interface Sci.* **253** 117
[102] Bock H and Schoen M 2000 *J. Phys.: Condens. Matter* **12** 1545
[103] Trokhymchuk A, Henderson D, Nikolov A D and Wasan D T 2001 *Langmuir* **17** 4940
[104] Richetti P and Kékicheff P 1992 *Phys. Rev. Lett.* **68** 1951

[105] Nikolov A D and Wasan D T 1989 *J. Colloid Interface Sci.* **133** 1
[106] Nikolov A D, Wasan D T, Denkov N D, Kralchevsky P A and Ivanov I B 1990 *Prog. Colloid Polym. Sci.* **82** 87
[107] Sonin A A and Langevin D 1993 *Europhys. Lett.* **22** 271
[108] Parker J L, Richetti P, Kékicheff P and Sarman S 1992 *Phys. Rev. Lett.* **68** 1955
[109] Bergeron V and Claesson P M 2002 *Adv. Colloid Interface Sci.* **96** 1
[110] Sedev R and Exerowa D 1999 *Adv. Colloid Interface Sci.* **83** 111
[111] Khristov K, Jachimska B, Malysa K and Exerowa D 2001 *Colloids Surf.* A **186** 93
[112] Guenoun P, Schalchli A, Sentenac D, Mays J W and Benattar J J 1995 *Phys. Rev. Lett.* **74** 3628
[113] von Klitzing R 2000 *Tenside Surf. Det.* **37** 338
[114] Kolaric B, Förster S and von Klitzing R 2001 *Prog. Colloid Polym. Sci.* **117** 195
[115] Rippner B, Boschkova K, Claesson P M and Arnebrant T 2002 *Langmuir* **18** 5213
[116] Ahrens H, Förster S and Helm C A 1998 *Phys. Rev. Lett.* **81** 4172
[117] Förster S, Hermsdorf N, Leube W, Schnablegger H, Regenbrecht M and Akari S J 1999 *Phys. Chem.* B **103** 6657
[118] Asnacios A, Espert A, Colin A and Langevin D 1997 *Phys. Rev. Lett.* **78** 4974
[119] von Klitzing R, Espert A, Asnacios A, Hellweg T, Colin A and Langevin D 1999 *Colloids Surf.* A **149** 131
[120] Kolaric B, Jaeger W and von Klitzing R 2000 *J. Phys. Chem.* B **104** 5096
[121] von Klitzing R, Espert A, Colin A and Langevin D 2001 *Colloids Surf.* A **176** 109
[122] Theodoly O, Tan J S, Ober R, Williams C E and Bergeron V 2001 *Langmuir* **17** 4910
[123] von Klitzing R, Kolaric B, Jaeger W and Brandt A 2002 *Phys. Chem. Chem. Phys.* **4** 1907
[124] Asnacios A, Langevin D and Argillier J F 1996 *Macromolecules* **29** 7412
[125] Asnacios A, von Klitzing R and Langevin D 2002 *Colloids Surf.* A **167** 189
[126] Stubenrauch C, Albouy P A, von Klitzing R and Langevin D 2000 *Langmuir* **16** 3206
[127] Taylor D J F, Thomas R K and Penfold J 2002 *Langmuir* **18** 4748
[128] Bergeron V, Langevin D and Asnacios A 1996 *Langmuir* **12** 1550
[129] von Klitzing R and Müller H J 2002 *Curr. Opin. Colloid Interface Sci.* **7** 18
[130] Kolaric B and von Klitzing R 2003 *J. Phys. Chem.* B submitted
[131] von Klitzing R and Kolaric B 2003 *Prog. Colloid Polym. Sci.* at press
[132] von Klitzing R and Kolaric B 2003 *Tenside Surf. Det.* submitted
[133] Hellweg T, Henry-Toulme N, Chambon M and Roux D 2000 *Colloids Surf.* A **163** 71
[134] Nierlich M, Williams C E, Boue F, Cotton J P, Daoud M, Farnoux B, Jannink G, Picot C, Moan M, Wolff C, Rinaudo M and de Gennes P G 1979 *J. Physique* **40** 701
[135] Förster S and Schmidt M 1995 *Adv. Polym. Sci.* **120** 51
[136] Nishida K, Kaji K and Kanaya T 1995 *Macromolecules* **28** 2472
[137] Essafi W, Lafuma F and Williams C E 1999 *Eur. Phys. J.* B **9** 261
[138] Claesson P M, Bergström M, Dedinaite A, Kjellin M, Legrand J F and Grillo I 2000 *J. Phys. Chem.* B **104** 11689
[139] de Gennes P G, Pincus P, Velasco R M and Brochard F 1976 *J. Physique* **37** 37
[140] Odijk T 1997 *J. Polym. Sci. Polym. Phys. Edn* **15** 688
[141] Skolnick J and Fixman M 1977 *Macromolecules* **10** 944
[142] Dobrynin A V, Colby R V and Rubinstein M 1995 *Macromolecules* **28** 1859
[143] Barrat J L and Joanny J F 1996 *Adv. Chem. Phys.* **94** 1
[144] Oosawa F 1957 *J. Polym. Sci.* **23** 421
[145] Manning G S 1969 *J. Chem. Phys.* **51** 924
[146] Ray J and Manning G S 1997 *Macromolecules* **30** 5739
[147] Khokhlov A R and Khachaturian K A 1982 *Polymer* **23** 1742
[148] Milling A J 1996 *J. Phys. Chem.* **100** 8986
[149] Milling A J and Vincent B 1997 *J. Chem. Soc. Faraday Trans.* **93** 3179
[150] Milling A J and Kendal K 2000 *Langmuir* **16** 5106
[151] Chatelier X and Joanny J F 1996 *J. Physique* II **6** 1669
[152] Yethiraj A 1999 *J. Chem. Phys.* **111** 1797
[153] Pfeuty P 1978 *J. Physique Coll.* **39** C2 149
[154] Khokhlov A R 1980 *J. Phys. A: Math. Gen.* **13** 979
[155] von Klitzing R and Langevin D unpublished results